In-situ electro-generation and activation of hydrogen peroxide using a CuFeNLDH-CNTs modified graphite cathode for degradation of cefazolin

Ghasemi, Masoumeh

Academic press
2020-08-01

Ghasemi, M, Khataee, A, Gholami, P, Soltani, R D C, Hassani, A & Orooji, Y 2020, 'In-situ electro-generation and activation of hydrogen peroxide using a CuFeNLDH-CNTs modified graphite cathode for degradation of cefazolin', Journal of Environmental Management, vol. 267, 110629. https://doi.org/10.1016/j.jenvman.2020.110629

http://hdl.handle.net/10138/346533
10.1016/j.jenvman.2020.110629

In-situ electro-generation and activation of hydrogen peroxide using a CuFeNLDH-CNTs modified graphite cathode for degradation of cefazolin

Masoumeh Ghasemi,[b] Alireza Khataee,[b, c, d*] Peyman Gholami,[b, e] Reza Darvishi Cheshmeh Soltani,[f] Aydin Hassani,[g] Yasin Orooji,[a,*]

[a] College of Materials Science and Engineering, Nanjing Forestry University, Nanjing 210037, China

[b] Research Laboratory of Advanced Water and Wastewater Treatment Processes, Department of Applied Chemistry, Faculty of Chemistry, University of Tabriz, 51666-16471 Tabriz, Iran

[c] Department of Environmental Engineering, Gebze Technical University, 41400 Gebze, Turkey

[d] Institute of Research and Development, Duy Tan University, Da Nang 550000, Vietnam

[e] Department of Chemistry, University of Helsinki, P.O. Box 55, Helsinki 00014, Finland

[f] Department of Environmental Health Engineering, School of Health, Arak University of Medical Sciences, 38196-93345 Arak, Iran

[g] Department of Materials Science and Nanotechnology Engineering, Near East University, 99138 Nicosia, TRNC, Mersin 10, Turkey

* Corresponding authors:

Email: a_khataee@tabrizu.ac.ir (A. Khataee)

yasin@njfu.edu.cn (Y. Orooji)

Abstract

The modified multifunctional electrodes for electro-Fenton (EF) process are suggested to be promising cathodes for in situ electro-generation and activation of H_2O_2 to produce hydroxyl radicals (•OH). However, heterogeneous EF process still faces the challenges of limited catalytic activity and releasing of massive amounts of transition metals to the solution after removal of organic pollutants. The main aim of the present investigation was to prepare a cathode containing carbon nanotubes (CNTs) and CuFe nano-layered double hydroxide (NLDH) for degradation and mineralization of cefazolin antibiotic through electro-Fenton process. Structural and electrochemical analyses demonstrated that CuFeNLDH-CNTs nanocomposite was successfully incorporated on the surface of graphite cathode. Due to the increased formation of •OH in the reactor, the incorporation of CNTs into NLDH matrix with a catalyst loading of 0.1 g substantially improved the degradation efficiency of cefazolin (89.9%) in comparison with CNTs-coated (28.7%) and bare graphite cathode (22.8%) within 100 min. In the presence of 15 mM of ethanol, the degradation efficiency of cefazolin was remarkably decreased to 43.7% by the process, indicating the major role of •OH in the destruction of target molecules. Acidic conditions favored the degradation efficiency of cefazolin by the modified EF process. Mineralization efficiency of the bio-refractory compound was obtained to be 70.1% in terms of chemical oxygen demand (COD) analysis after 300 min. The gas chromatography-mass spectroscopy (GC-MS) analysis was also implemented to identify the intermediate byproducts generated during the degradation of cefazolin in the CuFeNLDH-CNTs/EF reactor.

Keywords: Electrochemical advanced oxidation processes (EAOPs); Antibiotic compound; Layered double hydroxide; Carbon nanotubes; Fenton reaction.

1. Introduction

In recent years, the discharge of wastewaters containing pharmaceutical compounds into aquatic ecosystems has become a great environmental and health concern [1, 2]. Among various groups of pharmaceuticals, antibiotic compounds have been further considered because of their wide implementation for the treatment of bacterial-causing infections [3, 4]. A typical antibiotic model is cefazolin, which is a part of β-lactam cephalosporines antibiotics derived from the *Cephalosporium* fungus. It is a semi-synthetic compound manufactured for the treatment of acute infections in bones, stomach, heart valves and lungs [5, 6].

Noticeably, even trace amounts of β-lactam antibiotics such as cefazolin in water resources and wastewater treatment plants effluents may lead to adverse effect on aquatic life and subsequently human life [7, 8]. In addition, the presence of antibiotics such as cefazolin in the ecosystem will lead to the development of antibiotic-resistant microbial strains [9]. Microbial resistance against antibiotic drugs has become a major global health concern [10]. Since most antibiotics are categorized as recalcitrant compounds, biological treatment processes are not able to efficiently degrade this type of contaminants [11].

Application of efficient chemical treatment processes, especially advanced oxidation processes (AOPs) has been considered for effective destruction and mineralization of these bio-refractory compounds [12-14]. The implementation of AOPs results in the formation of hydroxyl radical ($^{\bullet}OH$) with high oxidation potential to non-selectively degrade various organic and inorganic substances [15]. Many AOPs have been examined for treating antibiotic compounds. Among them, due to their high effectiveness and low operational (annual) costs, Fenton-based treatment processes and in particular, Fenton's reaction-based electrochemical advanced oxidation processes (EAOPs) have been successfully utilized for the decontamination of antibiotic-polluted water streams [11, 16]. The efficiency of the electro-

74 Fenton (EF) process is significantly affected by the capability of the process to in situ generate
75 H_2O_2 through the cathodic reduction as shown in the following reaction [11]:

76 $$O_2 + 2H^+ + 2e^- \rightarrow H_2O_2 \quad (1)$$

77 In the following, the as-generated H_2O_2 molecules react with iron ions as Fenton catalyst to
78 produce $^{\bullet}OH$ in the bulk solution [17]:

79 $$Fe^{2+} + H_2O_2 + H^+ \rightarrow Fe^{3+} + {}^{\bullet}OH + H_2O \quad (2)$$

80 According to the previous studies, efficient generation of H_2O_2 in EF process can be
81 attained by the immobilization of carbonaceous nanostructures such as carbon nanotubes
82 (CNTs) on the graphite cathode surface [18, 19]. CNTs can offer important benefits for the
83 two-electron reduction of oxygen owing to their good surface activity, high electrical
84 conductivity, and mechanical strength [19]. On the other hand, as an innovative method, the
85 catalyst is immobilized on the cathode surface to continuously generate $^{\bullet}OH$ in the bulk
86 solution. Based on this approach, the stability of the EF process in repeated runs will be
87 increased as well as its cost-effectiveness. Iron ions are constantly regenerated on the surface
88 of the catalyst-coated cathode.

89 Layered double hydroxides (LDHs) are one of the most useful classes of inorganic layered
90 compounds which can be used to host heterogeneous Fenton catalysts on the surface of cathode,
91 improving its structure for the in-situ generation of H_2O_2 and subsequently, the formation of
92 $^{\bullet}OH$ during the EF process. Due to their versatility as well as their unique structure with high
93 porosity and thermal stability, LDHs and their modifications have been extensively utilized as
94 heterogeneous catalysts for numerous applications [20, 21].

95 In this study, Fe together with Cu ions was incorporated into LDH matrix as Fenton
96 reaction's catalysts to avoid the leachate of toxic Fe and Cu ions into the ecosystem.
97 Considering the advantages of nano-materials, the nano-LDH (NLDH) containing Fe and Cu

nanostructures was used as an active site to catalyze the generation of free oxidizing agents for the decomposition of target contaminants. CNTs were added to the CuFeNLDH-coated cathode to produce more oxidizing radicals in the solution for the degradation of cefazolin antibiotic. The as-synthesized cathode was characterized by using scanning electron microscopy (SEM), high resolution transmission electron microscopy (HR-TEM), X-ray diffraction (XRD), Fourier transform infrared spectroscopy (FT-IR), Energy-dispersive X-ray spectroscopy (EDX) equipped with elemental mapping, X-ray photoelectron spectroscopy (XPS), cyclic voltammetry (CV), and linear scan voltammetry (LSV) analyses. Hitherto, no study has been performed and reported regarding the application of CuFeNLDH/CNTs-coated graphite as nanocomposite cathode for the EF process to decontaminate polluted water streams. Chemical oxygen demand (COD) and gas chromatography-mass spectrometry (GC–MS) analyses were also performed to determine the mineralization rate and intermediate byproducts during the degradation of cefazolin.

2. Materials and methods

2.1. Chemicals

Copper (II) nitrate trihydrate ($Cu(NO_3)_2.3H_2O$: 90%), iron (III) nitrate hexahydrate ($Fe(NO_3)_3.6H_2O$: 99%), ammonium fluoride (NH_4F: 95%), hydrochloric acid (HCl: 37%), sodium sulfate (Na_2SO_4: 98.5%), hydrogen peroxide (H_2O_2: 35%), sodium carbonate (Na_2CO_3: 98%), nitric acid (HNO_3: 65%), sulfuric acid (H_2SO_4: 98%), ethanol (C_2H_5OH: 96%), urea (CH_4N_2O: 99.5%), 1,4-benzoquinone ($C_6H_4O_2$: 99%), n-butanol ($C_4H_{10}O$ > 99.7%) and sodium hydroxide (NaOH: 99%) were obtained from Merck (Germany). Pristine multi-walled carbon nanotubes (MWCNTs) with 3-5 nm inner diameter and 8-15 nm outer diameter were obtained from Cheap Tubes (USA). 60% polytetrafluoroethylene (PTFE) solution (Teflon

Dispersion, DISP 30) was purchased from DuPont (USA). Graphite plates were purchased from Tabriz Zoghal Co. (Iran). Cefazolin was obtained from Loghman Co. (Iran). The characteristics and chemical structure of cefazolin are presented in Table 1.

2.2. Modification of CNTs

For the addition of hydroxyl and carboxyl groups onto the surface of CNTs, a mixture of pristine CNTs and 1: 3 volume ratio of nitric acid and sulfuric acid were sonicated at 80.0 ± 0.5 ºC for 1 h. After washing with deionized water and centrifugation with 3500 ± 50 rpm for 30 min, the acid-treated CNTs were dried at 60.0 ± 0.5 °C for 12 h (Fig. S1).

2.3. Synthesis of CuFeNLDH-CNTs

The CuFeNLDH-CNTs nanocomposite was synthesized by the hydrothermal method. Appropriate amounts of $Cu(NO_3)_2.3H_2O$ (250.0 mmol/L), $Fe(NO_3)_3.6H_2O$ (125.0 mmol/L), NH_4F (312.5 mmol/L), Urea (1250.0 mol/L) and modified CNTs (0.5 g) were mixed in 70 mL deionized water. The resulting solution was stirred with a magnetic stirrer for 30 min. After that, the obtained solution was transferred into a 100 mL Teflon-lined stainless steel autoclave. The sealed autoclave was placed in an oven and kept at 90.0 ± 0.5 °C for 24 h. Finally, as-synthesized CuFeNLDH-CNTs crystals were dried at 50.0 ± 0.5 ºC after five times washing (Fig. S2).

2.4. Immobilization of CuFeNLDH-CNTs on the graphite plate

In order to clean the surface of the graphite plate, it was immersed in a solution of 10% nitric acid and sonicated using a probe sonicator (Hielscher, UP400S, 400 W, 24 kHz) for 30 min. Firstly, 1.4 g PTFE and 0.1 g CuFeNLDH-CNT were added to the mixture of water (30

mL) and n-butanol (6% w/w). The obtained suspension was sonicated for 30 min to obtain a highly dispersed mixture. The resulting mixture was heated at 80.0 ± 0.5 °C until an ointment appeared. The resulting ointment was immobilized on the graphite plate and was calcined at 350 ± 5 °C for 15 min under nitrogen gas. PTFE in the cathode has two roles: pasting the high surface CuFeNLDH-CNTs into a cohesive layer and imparting some hydrophobic character to the layer. Schematic diagram for the stabilization of nanocomposite on the graphite plate is shown in Fig. S3.

2.5. Characterization

XRD analysis (PANalytical X'Pert PRO, Germany) with Cu Kα radiation (λ = 0.15406 nm) was used to determine the crystallite structure of the treated graphite plate at 40 mA and 45 kV. The functional groups of CuFeNLDH, CNTs and CuFeNLDH-CNTs were analyzed by FT-IR spectrometer (Tensor 27, Bruker, Germany), with the KBr pellet in the range of 400–4000 cm^{-1}. The surface morphology, magnitudes and chemical composition of CuFeNLDH, CNTs, CuFeNLDH-CNTs and the treated graphite electrode were examined by SEM equipped with EDX spectroscopy (Mira3 FEG-SEM Tescan, Czech Republic). HR-TEM images were taken by a high resolution microscope (Hitachi HT-7700, Japan) operating at 120 kV. CV (scan rate of 50 mV/s) and LSV were performed using an electrochemical system (PG-Stat 30, Netherlands). XPS spectra were also recorded using Kratos AXIS UltraDLD spectrometer (UK).

2.6. Apparatus and analyses

For EF experiments, the anode was a platinum sheet (6.25 cm^2) and the cathode was the CuFeNLDH-CNTs-coated graphite plate (3 cm^2). The distance between the platinum sheet and

the treated graphite plate was 1 cm. EF experiments were done at room temperature (25.0 ± 0.5 °C) using an undivided cylindrical glass reactor containing 80 mL cefazolin-contained solution as the target pollutant and Na_2SO_4 as the supporting electrolyte with certain concentrations. Both electrodes were connected to a DC power supply (Adak PS-808, Iran). During the reaction time, an air pump (RS-510, China) was used for air injection into the reactor. Ozone gas (ozone generator, BE-72, Iran) was bubbled into the bulk solution by means of a porous diffuser. It was coupled with an oxygen concentrator (Airsep, USA). The cefazolin degradation was measured by determining the absorbance at a wavelength of 260 nm with a UV-Vis spectrophotometer (SU–6100, Philler scientific, USA). The concentration of H_2O_2 electro-generated on the surface of bare graphite electrode and modified electrodes were determined by the iodide method [22]. The COD concentration before the treatment process and the residual COD after the treatment process were determined by a standard method (method no. 5220) [23], using Palin test (United Kingdom) apparatus. The intermediates produced during the cefazolin degradation were determined by Agilent 6890 gas chromatography-mass spectrometry (GC–MS) and an Agilent 5973 mass spectrometer (Canada).

3. Results and discussion

3.1. Characterization

3.1.1. SEM images

Fig. 1 exhibits the SEM images of CuFeNLDH (a-d), pristine CNTs (e-h), CuFeNLDH-CNTs nanocomposite (i-l) and CuFeNLDH-CNTs-coated graphite cathode (m-p). As can be seen in Fig. 1 (a-d), CuFeNLDH consists of microspheres decorated with nano-sheets with an average diameter of 26 nm. The SEM images of CuFeNLDH-CNTs nanocomposite display that CNTs are successfully incorporated into CuFeNLDH nano-sheets (Fig. 1 (i-l)). CuFeNLDH-CNTs nanocomposite coated on graphite plate can be also observed in Fig. 1 (m-

p). The presence of nano-tubes in the structure of CuFeNLDH-CNTs nanocomposite immobilized on the surface of graphite cathode can be clearly seen in Fig. 1 (o and p).

3.1.2. EDX spectra

EDX spectroscopy equipped with SEM analysis was implemented to specify elemental composition of CuFeNLDH, CNTs, CuFeNLDH-CNTs and CuFeNLDH-CNTs-coated graphite cathode (Fig. S4 (a-d)). The results revealed that the CuFeNLDH contained O, N, C, Cu and Fe elements (Fig. S4 (a)). According to Fig. S4 (b), the CNTs is composed of C and O elements. Compared with non-immobilized CuFeNLDH-CNTs, the amount of C element in the structure of the modified cathode remarkably increased due to the immobilization of CuFeNLDH-CNTs on the surface of graphite cathode. The elemental mapping images of CuFeNLDH/CNTs-coated graphite cathode was also performed (Fig. S5). As shown, the elements in the composition of the modified cathode are uniformly distributed, indicating the suitable structure of as-synthesized cathode for the reduction of oxygen molecule and generation of $^{\bullet}OH$ via the whole surface of cathode through the interaction of Cu and Fe ions with electro-generated H_2O_2.

3.1.3. HR-TEM images

HR-TEM images of CuFeNLDH and CuFeNLDH-CNTs are exhibited in Fig. 2. Fig. 2 (a and b) indicates the formation of sheet-like CuFeNLDH nanostructures with regular size and relatively uniform size distribution. The size of thickness and width of CuFeNLDH nanostructures are in the range of 10.00-30.00 and 20.00-50.00 nm, respectively (Fig. 2 (e and f)). The images of CNTs-implanted CuFeNLDH show the presence of ultrafine structures in the composition of nanocomposite (Fig. 2 (c and d)), creating high surface area and more reaction sites for the generation of H_2O_2 molecules and $^{\bullet}OH$ radicals to catalytically convert

the target antibiotic pollutant. Fig. 2 (d) displays that CNTs are successfully introduced into the CuFeNLDH nano-sheets.

3.1.4. XRD patterns

The XRD patterns of CuFeNLDH, CuFeNLDH-CNTs, and CuFeNLDH-CNTs-coated graphite are shown in Fig. 3 (a-c). For the XRD pattern of CuFeNLDH (Fig. 3a), characteristic peaks placed at 12.8, 25.8, 33.6, 36.5 and 43.2° correspond to the (003), (006), (012), (015) and (018) crystal plane according to JCPDS card no. 41-1428 [24]. In the case of XRD patterns obtained for CuFeNLDH-CNTs (Fig.3b) and CuFeNLDH-CNTs-coated graphite (Fig.3c), the diffraction peak located at about 26.5° is associated with the (002) reflection of the CNTs and graphite based on JCPDS card no. 74-444 [25].

3.1.5. FT-IR spectra

The FT-IR spectra of CuFeNLDH, CNTs and CuFeNLDH-CNTs samples are displayed in Fig. S6. FT-IR spectrum of CuFeNLDH exhibits the peaks at 464 and 582 cm^{-1} attributed to the Fe-O vibration [26]. The peak placed at 518 cm^{-1} indicates the Cu-O bond [27]. A broad and intense peak was observed at 3452 cm^{-1}, related to the O-H stretching vibration [28, 29]. The weak peaks located at 2854 to 2925 cm^{-1} are ascribed to symmetric and asymmetric stretching of C-H bond, respectively [30]. Moreover, the peaks at 1386, 1687 and 875 cm^{-1} can be related to C-N, C=O and C-O vibrations, respectively [31, 32]. The peaks for C=O vibration (1645 cm^{-1}) and C-N vibration (1126 cm^{-1}) can be observed in the spectrum of the modified CNTs [33]. As mentioned, the peak at 3458 cm^{-1} represents the O-H group in the structure of CuFeNLDH-CNTs [34]. However, CuFeNLDH-CNTs spectrum shows an absorption band at 516 cm^{-1} attributed to Cu-O vibrations [26] and a peak at 680 cm^{-1} related to Fe-O vibration [35].

3.1.6. XPS

XPS analysis was performed for CuFeNLDH, CuFeNLDH/CNTs, and CuFeNLDH-CNTs-coated graphite cathode whose results are presented in Fig. 4. As can be seen in XPS full spectra of the samples (Fig. 4 (a-c)), CuFeNLDH is composed of O (39.53%), Cu (27.37%), Fe (15.71%), C (12.46%) and N (4.93%) elements. CuFeNLDH/CNTs sample contains O, Cu, Fe, C and N elements with 38.42, 18.82, 8.71, 30.13 and 3.92 atomic percent (At%), respectively. The higher At% of carbon in the structure of the modified cathode compared with CuFeNLDH/CNTs sample is owing to the immobilization of CuFeNLDH-CNTs on the surface of graphite cathode. It was found that the Fe/Cu At% ratio in CuFeNLDH, CuFeNLDH/CNTs, and CuFeNLDH-CNTs-coated graphite cathode was 0.57, 0.46 and 0.53 which is in good accordance with 1/2 molar ratio of iron/copper precursors utilized in the preparation of the samples. High-resolution XPS spectra of Fe 2p, Cu 2p and O 1s are shown in Fig. 4 (d-l). Fig. 4 (d and e) shows the presence of three peaks at ~712, ~719 and ~725 eV, which are attributed to Fe 2p1/2, Fe 2p3/2 and their satellite, demonstrating that the main part of iron in the structure of CuFeNLDH and CuFeNLDH/CNTs samples is in trivalent state [36]. After immobilizing CuFeNLDH/CNTs on the graphite surface, the peak at ~719 eV nearly disappeared and a new peak was observed at ~708 eV corresponding to Fe^{2+} ion (Fig. 4 (d-l)) [37]. This observation demonstrated that a part of Fe^{3+} in the structure of CuFeNLDH was reduced to Fe^{2+} during the calcination of the CuFeNLDH/CNTs-modified electrode at 350 ± 5 °C under nitrogen atmosphere. The Cu 2p XPS spectra of CuFeNLDH and CuFeNLDH/CNTs (Fig. 4 (g and h)) exhibit the peaks at ~935, ~942, ~955 and ~962 eV which illustrate copper oxidation state of 2+ [38]. Compared with CuFeNLDH and CuFeNLDH-CNTs, the intensities of the peaks observed in high-resolution spectrum of Fe 2p were considerably decreased for CuFeNLDH-CNTs-coated graphite (Fig. 4 (f)) and Cu 2p peaks became indistinguishable from background

noise (Fig. 4 (i)). This can be related to the immobilization of CuFeNLDH-CNTs on the graphite plate using PTFE binder which leads to a decrease in Fe and Cu contents and the variation of their surrounding electron density due to the presence of adjacent species [39, 40]. As shown in high-resolution XPS spectra of O 1s (Fig. 4 (j-l)), there is a single peak at binding energy of ~533 eV which can be ascribed to OH^- belonging to metal hydroxides or hydroxyl groups [41].

3.1.7. CV and LSV curves

The electrochemical performance of the bare graphite cathode was compared with graphite cathodes modified with CuFeNLDH/CNTs nanocomposite using cyclic voltammetry (CV) analysis. Fig. 5 (a) and (b) show the results of CV analysis carried out in the potential range of -0.7-1.0 V with a scan rate of 50.0 mV/s in N_2- and O_2-saturated solutions, respectively. A reduction peak was detected at the potential around –0.1 V in oxygen saturated solution. However, no obvious reduction peak was observed for N_2 saturated solution, and its reductive current was slightly lower than that of in O_2-saturated solution, revealing that the prepared cathodes had high activity toward oxygen reduction. On the other hand, the graphite cathodes modified with CuFeNLDH/CNTs nanocomposite have a higher oxygen evolution potential than that of the bare graphite cathode. Linear scan voltammetry (LSV) analysis was also used to further evaluate the electrochemical properties of the modified graphite cathodes in comparison with the bare cathode (Fig. 5 (c)). Accordingly, the results of LSV analysis verified the results of CV analysis. The high oxygen evolution potential of the cathodes leads to the increased generation of hydrogen peroxide and subsequently, increased $^{\bullet}OH$ in the bulk solution. Moreover, high oxygen evolution potential reduces power loss during the electrochemical-based treatment process, leading to the enhanced cost-effectiveness of the process and its current efficiency [42]. At a specified potential, lower increase in the current of

graphite cathodes modified with CuFeNLDH/CNTs nanocomposite was obtained in comparison with that of the bare cathode. The electroactive surface area of the electrodes were determined in the ferrocyanide system ($[Fe(CN)_6]^{3-}/[Fe(CN)_6]^{4-}$) based on the Randles-Sevcik equation (Eq. 3) [43]:

$$I_p = 2.69 \times 10^5 \times AD^{1/2}n^{3/2}\gamma^{1/2}C \quad (3)$$

where Ip is the peak current (A), A is the geometric area of the electrode (cm^2), D is the diffusion coefficient of the probe molecule (7.60×10^{-6} cm^2 s^{-1}), C is the concentration of $[Fe(CN)_6]^{4-}$ in solution (1×10^{-5} mol/cm^{-3}), n = 1 is the number of electrons involved in the redox Fe^{III}/Fe^{II} reaction and γ is the scan rate (0.05 V s−1). As displayed in Fig. 5 (b), the peak currents of both graphite/CNTs (0.1 g) and graphite/NLDH-CNTs (0.1 g), were higher than that of bare graphite cathode. Accordingly, electroactive surface area was calculated as 5.61, 8.82 and 8.29 for the bare graphite, graphite/CNTs (0.1 g) and graphite/NLDH-CNTs (0.1 g), respectively. The electroactive surface area is one of the important characteristics of the cathode that can potentially enhance the efficiency of the EF process in terms of hydrogen peroxide generation.

3.2. Comparison of the performance of different electrodes

A comparative study was performed before the evaluation of the effect of the main operational parameters on the efficiency of the treatment process. The results of these preliminary experiments are provided in Fig. 6 (a). Based on the data obtained, the immobilization of CNTs on the surface of the bare cathode resulted in an insignificant increase in the degradation efficiency of cefazolin compared with the bare cathode (increasing from 22.8% to 28.7%). Interestingly, an obvious increase in the degradation of cefazolin occurred when the CNTs were incorporated into CuFeNLDH lattice. Due to the facile interchangeability of implanted anions and uniform distribution of metal cations in the brucite-like layers of the

compound, LDHs exhibit catalytic activity as semiconductor with high stability to be used in various systems including catalytic treatment processes [44]. Particularly, Fe together with Cu ions which are incorporated into LDH matrix act as Fenton reaction's catalysts [20]; thus, the presence of these ions in the structure of LDH leads to the formation of •OH through the interaction with as-generated H_2O_2 molecules, which resulted in the enhanced degradation efficiency of cefazolin antibiotic by the electro-Fenton process in comparison with the application of CNTs alone. However, an optimum amount of CuFeNLDH-CNTs nanocomposite immobilized on the cathode surface is required to attain the maximum efficiency. The degradation efficiency of cefazolin increased from 48.0% to 69.8% when the amount of CuFeNLDH-CNTs increased from 0.05 to 0.10 g, respectively; while increasing the amount of CuFeNLDH-CNTs up to 0.15 g led to a slight decrease in the degradation efficiency of the pollutant (66.3%). Although the efficiency of CuFeNLDH/CNTs-equipped electro-Fenton process for the degradation of target compound can be enhanced by increasing the amount of coated catalyst; however, increasing the amount of CuFeNLDH/CNTs may cause mass transfer limitation on the cathode surface [45], leading to the reduced formation of oxidizing agents in the electrochemical cell. Moreover, the aggregation of coated catalyst on the surface of the cathode is inevitable at higher amounts which may be the dominating factors leading to the loss of catalyst [46]. Overall, the agglomeration of catalyst or increasing the thickness of the coated catalyst leads to the reduced reactive sites for the reduction of diffused oxygen molecules. Furthermore, protons with small size and high mobility can permeate into the thin film of the catalyst better than the thick layer [47]. Therefore, in the present study, the catalyst loading of 0.10 g was considered as the optimum value in comparison with other values (0.05 and 0.15 g) considering economic and applicability point of view. Fig. 6 (b) shows the concentration of H_2O_2 produced during the EF process on the bare graphite cathode, CNTs-coated graphite and graphite cathodes modified with different amounts of CuFeNLDH/CNTs

nanocomposite. Comparatively, the amount of electro-generated H_2O_2 decreased when the cathode surface was coated with CuFeNLDH/CNTs in comparison with the bare and CNTs-coated graphite. This can be due to the interaction of electro-generated H_2O_2 with Fe and Cu ions in the structure of NLDH, thereby producing $^{\bullet}OH$ and $HO_2^{\bullet}$ radicals in the solution for the efficient degradation of cefazolin according to Eqs. (4-7) [48]:

$$Fe^{3+} + H_2O_2 \rightarrow Fe^{2+} + HO_2^{\bullet} + H^+ \quad (4)$$

$$Fe^{2+} + OH^{\bullet} \rightarrow Fe^{3+} + OH^- \quad (5)$$

$$Cu^{2+} + H_2O_2 \rightarrow Cu^{+} + HO_2^{\bullet} + H^+ \quad (6)$$

$$Cu^{+} + H_2O_2 \rightarrow Cu^{2+} + OH^{-} + OH^{\bullet} \quad (7)$$

Based on the above reactions, the presence of CuFeNLDH on the cathode surface inhibits the accumulation of H_2O_2 molecules in the bulk solution. During the EF process, recycling potential of iron species can easily take place through the following equation:

$$Fe(III) + e^- \rightarrow Fe(II) \quad (8)$$

As-converted Fe(II) can directly react with hydrogen peroxide to produce $^{\bullet}OH$ radicals and concurrently be converted to Fe(III) ions. That is why the major oxidizing agent in the CuFeNLDH-CNTs/EF reactor was still $^{\bullet}OH$ radicals. It should not be overlooked that part of hydrogen peroxide molecules may be oxidized on the surface of Pt anode, generating oxygen molecules in the EF reactor [49]:

$$H_2O_2 \rightarrow O_2 + 2H^+ + 2e^- \quad (9)$$

3.3. Effect of operational parameters

370 The effect of initial pH on the degradation efficiency of cefazolin is displayed in Fig. 7 (a).
371 As shown, the acidic conditions favored the removal of target pollutant by the CuFeNLDH-
372 CNTs/EF process. An increase in the initial pH from 3.0 to 11.0 led to a decrease in removal
373 efficiency from 95.8% to 53.3%, respectively. Actually, the formation of hydrogen peroxide
374 through cathodic reduction is increased under acidic conditions, thereby leading to enhanced
375 production of $^{\bullet}OH$ in the CuFeNLDH-CNTs/EF reactor. Based on Fig. 7 (a), the change in the
376 degradation efficiency of cefazolin was not significant in the pH range of 3.0-6.0 (decreasing
377 from 95.8% to about 90.0%); thus, the pH value of 6.0 was chosen as the selective pH for
378 conducting the rest of the experiments, while taking cost-efficiency of the treatment system
379 into account. The effect of the applied current on the degradation efficiency of cefazolin by the
380 EF process was assessed (Fig. 7 (b)). Obviously, increasing the applied current in the range of
381 150.0-400.0 mA resulted in the enhanced degradation efficiency of cefazolin from 39.7% to
382 92.8% over the reaction time of 100 min. However, as shown in Fig. 7 (b), increasing the
383 current from 300.0 to 400.0 mA did not significantly influence the efficiency of the EF process
384 (not more than 3.0% increase in the degradation efficiency). In fact, the efficiency of the
385 process operated at these two applied currents was almost the same. Thus, the current intensity
386 of 300.0 mA was considered in the following experimental runs. The application of higher
387 applied currents results in the in-situ generation of more free radicals through the
388 CuFeNLDH/CNTs-coated graphite cathode [50]. Furthermore, increasing the current intensity
389 quickens the diffusion rate of the reactants in the bulk solution, bringing about the improved
390 efficiency of the EF reactor. The results of the effect of cefazolin concentration on its
391 degradation efficiency are presented in Fig. 7 (c). As a result, the degradation efficiency
392 decreased from 45.78% to 95.5% as the initial concentration of cefazolin decreased from 40.0
393 to 10.0 mg/L, respectively. Clearly, higher amounts of oxidizing agents are required to treat
394 the solution containing higher concentrations of cefazolin to attain the pre-determined

efficiency [51]. The effect of supporting electrolyte concentration on the degradation efficiency of cefazolin was also examined by varying the sodium sulfate concentration in the range of 25.0-100.0 mmol/L. According to Fig. 7 (d), rapid increase in the degradation efficiency of cefazolin from 59.5% to about 90.0% was observed when the supporting electrolyte concentration increased from 25.0 to 50.0 mmol/L; while, increasing its concentration from 50.0 to 75.0 mmol/L did not meaningfully influence the efficiency of the EF process over the reaction time of 100 min. Noticeably, increasing the electrolyte concentration from 75.0 to 100.0 mmol/L led to a substantial decrease in the degradation efficiency of cefazolin from 92.7% to 82.2%, respectively. It can be deduced that the amount of supporting electrolyte should be optimized to operate the treatment process cost-efficiently for full-scale applications. Considering the importance of this issue, the electrolyte concentration of 50.0 mmol/L was chosen for conducting the next experiments.

3.4. Effect of scavenging compounds

The effect of some main scavenging compounds on the degradation efficiency of cefazolin by the CuFeNLDH-CNTs/EF process was evaluated to specify not only the efficiency of the process under adverse conditions but also to determine the role of free oxidizing species in the degradation of target contaminants (Fig. 8). In this regard, inorganic (sodium carbonate) and organic (ethanol (EtOH) and benzoquinone (BQ)) scavenging compounds in the concentration range of 5.0-15.0 mmol/L were added to the cefazolin-contained solution to assess the change in the efficiency of the CuFeNLDH-CNTs/EF process. As illustrated in Fig. 8 (a), the presence of ethanol ($^{\bullet}OH$ scavenger) remarkably reduced the degradation efficiency of cefazolin by the EF process according to the following equation [52]:

$$^{\bullet}OH + C_2H_5OH \rightarrow H_2O + CH_3CHOH^{\bullet} \quad (10)$$

At ethanol concentrations of 5.0, 10.0 and 15.0 mmol/L, the degradation efficiencies of 62.3%, 53.1% and 43.7% were obtained, respectively; while in the absence of ethanol the degradation efficiency of about 90.0% was achieved within 100 min. The presence of BQ ($O_2^{\bullet-}$ scavenger) led to the decreased degradation efficiency of cefazolin (Fig. 8 (b)). The scavenging characteristic of BQ is represented through the following equation [53]:

$$BQ + O_2^{\bullet-} \rightarrow O_2 + BQ^{\bullet-} \quad (11)$$

BQ is recognized as high potential superoxide anions ($O_2^{\bullet-}$) scavenger [54]. At BQ concentrations of 5.0, 10.0 and 15.0 mmol/L, the degradation efficiencies of 76.0%, 69.7% and 59.1% were obtained, respectively. Results of the effect of carbonate ions on the degradation efficiency of cefazolin are displayed in Fig. 8 (c). The decreased degradation efficiency of cefazolin in the presence of carbonate ions is associated with its reaction with $^{\bullet}OH$ radical to produce carbonate radicals with lower oxidation potential as represented in the equation below [17]:

$$^{\bullet}OH + CO_3^{2-} \rightarrow CO_3^{\bullet-} + OH^- \quad (12)$$

The degradation efficiency of cefazolin decreased from 90.0% to 80.3%, 69.7% and 51.5% in the presence of 5.0, 10.0 and 15.0 mmol/L sodium carbonate, respectively. Based on the results obtained, the presence of ethanol led to the most suppressing effect on the degradation of cefazolin through the CuFeNLDH-CNTs/EF process in comparison with both BQ molecules and carbonate ions. Considering $^{\bullet}OH$ radical scavenging properties of ethanol, indicating the major role of $^{\bullet}OH$ radical in the degradation of antibiotic molecules through the EF process [55], shows that the result is consistent with those obtained and deduced at the end of preliminary experiments data section.

3.5. Gas injection

Fig. 9 shows the effect of air, O_2, O_3, and Ar injected into the solution on the efficiency of the CuFeNLDH-CNTs/EF process. The addition of O_2 and O_3 enhanced the degradation of cefazolin through the EF process, while Ar sparging led to a significant drop in the degradation efficiency of cefazolin compared with the addition of air. Clearly, the injection of pure oxygen into the bulk solution leads to highly efficient electro-generation of hydrogen peroxide and its conversion to •OH radical in comparison with ambient air. Furthermore, oxygen molecules dissolved in the solution react with Fe ions, generating superoxide anions [56]. As previously mentioned, the addition of BQ demonstrated the role of this type of free radical, but to a lesser extent than •OH radical, in degrading the target pollutant. The highest degradation efficiency was attained when ozone gas was injected into the EF reactor. The interaction of ozone molecules with electro-generated hydrogen peroxide produces •OH radicals in the solution. Furthermore, the rest of as-generated hydrogen peroxide is dissolved in the liquid phase and dissociates into hydroperoxide (HO_2^-) anions, initiating a radical chain reaction to form extra •OH radicals thanks to the reaction with ozone gas [57]. Similar results have been reported by Shen et al. in the case of the catalytic decolorization of wastewater through the ozone/Fenton treatment process [58]. From another point of view, when ozone is injected into the CuFeNLDH-CNTs-equipped EF reactor, recycled Fe^{2+} play catalytic role for the conversion of ozone to •OH radical. The catalytic reaction of ozone with Fe ions also produces FeO^{2+} species, which gradually changes to •OH radical [59]:

$$Fe^{2+} + O_3 \rightarrow FeO^{2+} + O_2 \quad (13)$$

$$FeO^{2+} + H_2O \rightarrow Fe^{3+} + {}^{\bullet}OH + OH^- \quad (14)$$

3.6. COD, GC-MS, AAS and stability studies

The progress in the mineralization of the target bio-refractory compound was checked via COD analysis over the reaction time of 300 min. Under current intensity of 300.0 mA, the initial COD of the cefazolin-contained solution decreased from 264 mg/L to 79 mg/L by the CuFeNLDH-CNTs/EF process (mineralization efficiency of 70.1%). This result indicated the acceptable destruction and mineralization of the cefazolin antibiotic when it was treated through the CuFeNLDH-CNTs/EF process. The enhanced degradation and mineralization of cefazolin in the EF process equipped with CuFeNLDH-CNTs-coated graphite cathode were mainly the result of the improved catalytic degradation capability of the Fenton process [49]. Moreover, the efficient mineralization of the cefazolin improves the potential of the effluent to be treated by the subsequent biological system as a post-treatment method with environmentally friendly effluent. However, the degradation of the target organic compound may result in the formation of unknown organic and inorganic compounds. Thus, GC-MS analysis was carried out to identify the intermediate byproducts generated during the destruction of cefazolin through the CuFeNLDH-CNTs/EF process. The results of GC-MS analysis are displayed in Table 3. According to the byproducts listed in Table 3, cefazolin can be degraded by cleavage of C-S, N=N, N-N, C-N and C-C bonds. In the first step, the parent molecule was disintegrated to hydroxylated cyclic hydrocarbons such as 2-(3-isopropenyl-4-methyl-4-vinylcyclohexyl)-2-propanol, (NE)-N-(2-methyl-5-prop-1-en-2-ylcyclohex-2-en-1-ylidene) hydroxylamine and 2-ethylcyclohexan-1-ol. In the next step, (2E)-3,7-dimethylocta-2,6-dien-1-ol, Octan-4-ol and pentan-2-ol were produced as hydroxylated aliphatic compounds derived from the ring cleavage. Then, various short-chain aliphatic carboxylic acids such as propan-2-ol, 1,1-bis(methylsulfanyl)ethane, acetic acid, 2-hydroxyacetaldehyde and acetamide were produced as the final intermediates. According to the results reported by Le et al., the formation of short-chain aliphatic compounds can result in the detoxification of solution [60]. Using evolution of inhibition ratio, they have demonstrated that the toxicity is closely

associated with the existence of aromatic compounds at the early step of the degradation process rather than short-chain aliphatic compounds detected at the end of the EF process which have insignificant toxicity. Eventually, all of these compounds could be converted to carbon dioxide and water as the final products to achieve mineralization [61]. The AAS technique was also applied to determine the total concentration of Fe and Cu ions dissolved in the cefazolin-contained solution during the CuFeNLDH-CNTs/EF process. The AAS analysis results revealed the release of Fe (0.21 mg/L) and Cu (0.34 mg/L) ions from the modified graphite cathode into the solution during the treatment process. The stability of the CuFeNLDH-CNTs-coated graphite cathode was also investigated by performing ten consecutive experiments. After each experiment, the cathode was washed with distilled water and dried at room temperature. Then, the next experiment was performed under the same experimental conditions. As presented in Fig. S7, there is no remarkable decrement in the performance of CuFeNLDH-CNTs-coated graphite cathode after ten experiments, confirming high stability of the CuFeNLDH-CNTs-modified cathode for the EF process. No more than 4.0% reduction in the removal efficiency of cefazolin was observed at the end of tenth run. This improves the potential of the treatment process to be used in full-scale applications with considerable cost-effectiveness.

4. Conclusion

CNTs-incorporated CuFeNLDH was immobilized on the surface of the graphite plate to be efficiently applied as a porous cathode for the degradation of cefazolin antibiotic through the EF process. Characterization analyses proved the superior structure of CuFeNLDH/CNTs-coated graphite in comparison with both bare and CNTs-coated cathodes for the reduction of oxygen molecules to hydrogen peroxide as well as decomposition of hydrogen peroxide to $^{\bullet}OH$

radicals. Increasing the current intensity and supporting electrolyte concentration led to the enhanced destruction of cefazolin through the modified EF process. Conversely, increasing the initial cefazolin concentration along with increasing solution pH resulted in decreased decomposition efficiency. Evaluation of the efficiency of the treatment process in the presence of radical scavenging compounds demonstrated the major role of free oxidizing radicals, especially $^{\bullet}OH$ radicals, in the degradation of the target contaminant. These results also showed the high potential of the treatment process to be operated under real conditions. The treatment process had relatively high potential in mineralization of the bio-refractory antibiotic with the release of low amounts of Cu and Fe ions into the bulk solution. The results of GC-MS analysis confirmed the acceptable progress in the conversion of parent compound into the intermediates with low molecular weight and simple structure. Overall, the EF process equipped with CuFeNLDH/CNTs-coated graphite cathode can be utilized as one of the promising Fenton-based AOPs for the decontamination of antibiotic-polluted water streams before being discharged into various ecosystems.

Acknowledgements

The authors wish to thank the University of Tabriz (Project No: 825, 97.3.5), Nanjing Forestry University (Grant Nos. 163020139, 163020210, 163040109 and 163020236) and Science and Technology Department of Jiangsu Province (BK2020043008) for the support provided.

References

[1] P. Gholami, L. Dinpazhoh, A. Khataee, A. Hassani, A. Bhatnagar, Facile hydrothermal synthesis of novel Fe-Cu layered double hydroxide/biochar nanocomposite with enhanced sonocatalytic activity for degradation of cefazolin sodium, Journal of hazardous materials, 381 (2020) 120742.

[2] J. Wang, M. Y. Zhang, J. Liu, X. M. Hu, B. S. He, Using a targeted ecopharmacovigilance intervention to control antibiotic pollution in a rural aquatic environment. Science of The Total Environment, 696 (2019) 134007.

[3] S. Agarwal, I. Tyagi, V.K. Gupta, M. Sohrabi, S. Mohammadi, A.N. Golikand, A. Fakhri, Iron doped SnO_2/Co_3O_4 nanocomposites synthesized by sol-gel and precipitation method for metronidazole antibiotic degradation, Materials Science and Engineering: C, 70 (2017) 178-183.

[4] S. Zhang, I. Khan, X. Qin, K. Qi, Y. Liu, S. Bai, Construction of 1D Ag-AgBr/AlOOH Plasmonic Photocatalyst for Degradation of Tetracycline Hydrochloride, Frontiers in chemistry, 8 (2020) 117.

[5] Y.Y. Gurkan, N. Turkten, A. Hatipoglu, Z. Cinar, Photocatalytic degradation of cefazolin over N-doped TiO_2 under UV and sunlight irradiation: Prediction of the reaction paths via conceptual DFT, Chemical Engineering Journal, 184 (2012) 113-124.

[6] M. Liu, H. Ni, L. Yang, G. Chen, X. Yan, X. Leng, P. Liu, X. Li, Pretreatment of swine manure containing β-lactam antibiotics with whole-cell biocatalyst to improve biogas production, Journal of Cleaner Production, 240 (2019) 118070.

[7] K.A. Rickman, S.P. Mezyk, Kinetics and mechanisms of sulfate radical oxidation of β-lactam antibiotics in water, Chemosphere, 81 (2010) 359-365.

[8] M.K. Dail, S.P. Mezyk, Hydroxyl-radical-induced degradative oxidation of β-lactam antibiotics in water: Absolute rate constant measurements, The Journal of Physical Chemistry A, 114 (2010) 8391-8395.

563 [9] P. K. Thai, V. N. Binh, P. H. Nhung, P. T. Nhan, N. Q. Hieu, N. T. Dang, N. K. B. Tam,
564 N. T. K. Anh, Occurrence of antibiotic residues and antibiotic-resistant bacteria in effluents of
565 pharmaceutical manufacturers and other sources around Hanoi, Vietnam. Science of the Total
566 Environment, 645 (2018) 393-400.
567 [10] R.D.C. Soltani, M. Mashayekhi, M. Naderi, G. Boczkaj, S. Jorfi, M. Safari, Sonocatalytic
568 degradation of tetracycline antibiotic using zinc oxide nanostructures loaded on nano-cellulose
569 from waste straw as nanosonocatalyst, Ultrasonics Sonochemistry, 55 (2019) 117-124.
570 [11] V. Poza-Nogueiras, E. Rosales, M. Pazos, M.Á. Sanromán, Current advances and trends
571 in electro-Fenton process using heterogeneous catalysts – A review, Chemosphere, 201 (2018)
572 399-416.
573 [12] T. X. H. Le, L. F. Dumée, S. Lacour, M. Rivallin, Z. Yi, L. Kong, M. Bechelany, M.
574 Cretin, Hybrid graphene-decorated metal hollow fibre membrane reactors for efficient electro-
575 Fenton-Filtration co-processes. Journal of membrane science, 587 (2019) 117182.
576 [13] R. Darvishi Cheshmeh Soltani, A.R. Khataee, M. Mashayekhi, Photocatalytic degradation
577 of a textile dye in aqueous phase over ZnO nanoparticles embedded in biosilica
578 nanobiostructure, Desalination and Water Treatment, 57 (2016) 13494-13504.
579 [14] K. Qi, S.-y. Liu, A. Zada, Graphitic carbon nitride, a polymer photocatalyst, Journal of the
580 Taiwan Institute of Chemical Engineers, (2020). https://doi.org/10.1016/j.jtice.2020.02.012
581 [15] J. Gao, Y. Liu, X. Xia, L. Wang, L. Shao, T. Cai, W. Dong, Mechanisms for photo assisted
582 Fenton of synthesized pyrrhotite at neutral pH, Applied Surface Science, 463 (2019) 863-871.
583 [16] T. X. H. Le, M. G. Cowan, M. Drobek, M. Bechelany, A. Julbe, M. Cretin, Fe-nanoporous
584 carbon derived from MIL-53 (Fe): A heterogeneous catalyst for mineralization of organic
585 pollutants, Nanomaterials, 9 (2019) 641.
586 [17] W. Jiang, P. Tang, S. Lu, Y. Xue, X. Zhang, Z. Qiu, Q. Sui, Comparative studies of
587 H_2O_2/Fe(II)/formic acid, sodium percarbonate/Fe(II)/formic acid and calcium

588 peroxide/Fe(II)/formic acid processes for degradation performance of carbon tetrachloride,
589 Chemical Engineering Journal, 344 (2018) 453-461.
590 [18] H. Yang, M. Zhou, W. Yang, G. Ren, L. Ma, Rolling-made gas diffusion electrode with
591 carbon nanotube for electro-Fenton degradation of acetylsalicylic acid, Chemosphere, 206
592 (2018) 439-446.
593 [19] Y. Liu, Q. Fan, J. Wang, Zn-Fe-CNTs catalytic in situ generation of H_2O_2 for Fenton-like
594 degradation of sulfamethoxazole, Journal of hazardous materials, 342 (2018) 166-176.
595 [20] C. Li, G. Zhao, T. Zhang, T. Yan, C. Zhang, L. Wang, F. Jiao, A novel Ag@ TiON/CoAl-
596 layered double hydroxide photocatalyst with enhanced catalytic memory activity for removal
597 of organic pollutants and Cr (VI), Applied Surface Science, 504 (2020) 144352.
598 [21] S.O. Ganiyu, T.X. Huong Le, M. Bechelany, N. Oturan, S. Papirio, G. Esposito, E. van
599 Hullebusch, M. Cretin, M.A. Oturan, Electrochemical mineralization of sulfamethoxazole over
600 wide pH range using FeIIFeIII LDH modified carbon felt cathode: Degradation pathway,
601 toxicity and reusability of the modified cathode, Chemical Engineering Journal, 350 (2018)
602 844-855.
603 [22] N.V. Klassen, D. Marchington, H.C. McGowan, H_2O_2 determination by the I3-method
604 and by $KMnO_4$ titration, Analytical Chemistry, 66 (1994) 2921-2925.
605 [23] I. Talinli, G.J.W.r. Anderson, Interference of hydrogen peroxide on the standard COD test,
606 26 (1992) 107-110.
607 [24] H. Liu, Q. Jiao, Y. Zhao, H. Li, C. Sun, X. Li, Cu/Fe hydrotalcite derived mixed oxides as
608 new catalyst for thermal decomposition of ammonium perchlorate, Materials Letters, 64 (2010)
609 1698-1700.
610 [25] Z. Ai, H. Xiao, T. Mei, J. Liu, L. Zhang, K. Deng, J. Qiu, Electro-Fenton degradation of
611 rhodamine B based on a composite cathode of Cu_2O nanocubes and carbon nanotubes, The
612 Journal of Physical Chemistry C, 112 (2008) 11929-11935.

613 [26] K. Nagase, Y. Zheng, Y. Kodama, J. Kakuta, Dynamic study of the oxidation state of
614 copper in the course of carbon monoxide oxidation over powdered CuO and Cu_2O, Journal of
615 Catalysis, 187 (1999) 123-130.
616 [27] I.C. Pereira, A.S. Duarte, A.S. Neto, J.M.F. Ferreira, Chitosan and polyethylene glycol
617 based membranes with antibacterial properties for tissue regeneration, Materials Science and
618 Engineering: C, 96 (2019) 606-615.
619 [28] Z. Li, J. Xiao, C. Chen, L. Zhao, Z. Wu, L. Liu, D. Cai, Promoting desert biocrust
620 formation using aquatic cyanobacteria with the aid of MOF-based nanocomposite, Science of
621 The Total Environment, (2019) 134824. https://doi.org/10.1016/j.scitotenv.2019.134824.
622 [29] M. Safari, A. Khataee, R. Darvishi Cheshmeh Soltani, R. Rezaee, Ultrasonically facilitated
623 adsorption of an azo dye onto nanostructures obtained from cellulosic wastes of broom and
624 cooler straw, Journal of Colloid and Interface Science, 522 (2018) 228-241.
625 [30] M. B. Khan, X. Cui, G. Jilani, U. Lazzat, A. Zehra, Y. Hamid, B. Hussain, L. Tang, X.
626 Yang, Z. He, Eisenia fetida and biochar synergistically alleviate the heavy metals content
627 during valorization of biosolids via enhancing vermicompost quality, Science of the Total
628 Environment, 684 (2019) 597-609.
629 [31] C.-S. Wu, Y.-L. Liu, K.-Y. Hsu, Maleimide-epoxy resins: preparation, thermal properties,
630 and flame retardance, Polymer, 44 (2003) 565-573.
631 [32] K. Fang, M. Chen, J. Chen, Q. Tian, C. P. Wong, Cotton stalk-derived carbon fiber@ Ni-
632 Al layered double hydroxide nanosheets with improved performances for supercapacitors,
633 Applied Surface Science, 475 (2019) 372-379.
634 [33] S. Mondal, P. Chakraborty, P. Bairi, D.P. Chatterjee, A.K. Nandi, Light induced E–Z
635 isomerization in a multi-responsive organogel: elucidation from 1 H NMR spectroscopy,
636 Chemical Communications, 51 (2015) 10680-10683.

637 [34] R. Darvishi Cheshmeh Soltani, A.R. Khataee, H. Godini, M. Safari, M.J. Ghanadzadeh,
638 M.S. Rajaei, Response surface methodological evaluation of the adsorption of textile dye onto
639 biosilica/alginate nanobiocomposite: thermodynamic, kinetic, and isotherm studies,
640 Desalination and Water Treatment, 56 (2015) 1389-1402.
641 [35] C. Chen, J. Qu, C. Cao, F. Niu, W. Song, CuO nanoclusters coated with mesoporous SiO
642 2 as highly active and stable catalysts for olefin epoxidation, Journal of Materials Chemistry,
643 21 (2011) 5774-5779.
644 [36] Z. Li, M. Shao, H. An, Z. Wang, S. Xu, M. Wei, D.G. Evans, X. Duan, Fast
645 electrosynthesis of Fe-containing layered double hydroxide arrays toward highly efficient
646 electrocatalytic oxidation reactions, Chemical science, 6 (2015) 6624-6631.
647 [37] M. Wang, T. Hou, Z. Shen, X. Zhao, H. Ji, MOF-derived Fe_2O_3: Phase control and effects
648 of phase composition on gas sensing performance, Sensors and Actuators B: Chemical, 292
649 (2019) 171-179.
650 [38] J. Li, Q. Fan, Y. Wu, X. Wang, C. Chen, Z. Tang, X. Wang, Magnetic polydopamine
651 decorated with Mg–Al LDH nanoflakes as a novel bio-based adsorbent for simultaneous
652 removal of potentially toxic metals and anionic dyes, Journal of Materials Chemistry A, 4
653 (2016) 1737-1746.
654 [39] J. Tang, J. Wang, Iron-copper bimetallic metal-organic frameworks for efficient Fenton-
655 like degradation of sulfamethoxazole under mild conditions, Chemosphere, 241 (2020)
656 125002.
657 [40] X. Yang, L. Liu, M. Zhang, W. Tan, G. Qiu, L. Zheng, Improved removal capacity of
658 magnetite for Cr(VI) by electrochemical reduction, Journal of Hazardous Materials, 374 (2019)
659 26-34.

660 [41] Z. Lv, S. Yang, H. Zhu, L. Chen, N.S. Alharbi, M. Wakeel, A. Wahid, C. Chen, Highly
661 efficient removal of As (V) by using NiAl layered double oxide composites, Applied Surface
662 Science, 448 (2018) 599-608.
663 [42] M. Li, C. Feng, W. Hu, Z. Zhang, N. Sugiura, Electrochemical degradation of phenol using
664 electrodes of Ti/RuO_2–Pt and Ti/IrO_2–Pt, Journal of hazardous materials, 162 (2009) 455-462.
665 [43] F. Deng, H. Olvera-Vargas, O. Garcia-Rodriguez, Y. Zhu, J. Jiang, , S. Qiu, J. Yang,
666 Waste-wood-derived biochar cathode and its application in electro-Fenton for sulfathiazole
667 treatment at alkaline pH with pyrophosphate electrolyte. Journal of Hazardous Materials, 377
668 (2019) 249-258.
669 [44] G. Fan, F. Li, D.G. Evans, X. Duan, Catalytic applications of layered double hydroxides:
670 recent advances and perspectives, Chemical Society Reviews, 43 (2014) 7040-7066.
671 [45] M. Wang, M. Chen, Z. Yang, G. Liu, J. Kee Lee, W. Yang, X. Wang, High-performance
672 and durable cathode catalyst layer with hydrophobic C@PTFE particles for low-Pt loading
673 membrane assembly electrode of PEMFC, Energy Conversion and Management, 191 (2019)
674 132-140.
675 [46] L. Qu, Z. Wang, X. Guo, W. Song, F. Xie, L. He, Z. Shao, B. Yi, Effect of electrode Pt-
676 loading and cathode flow-field plate type on the degradation of PEMFC, Journal of Energy
677 Chemistry, 35 (2019) 95-103.
678 [47] Z. Kang, G. Yang, J. Mo, Y. Li, S. Yu, D.A. Cullen, S.T. Retterer, T.J. Toops, G. Bender,
679 B.S. Pivovar, J.B. Green, F.-Y. Zhang, Novel thin/tunable gas diffusion electrodes with ultra-
680 low catalyst loading for hydrogen evolution reactions in proton exchange membrane
681 electrolyzer cells, Nano Energy, 47 (2018) 434-441.
682 [48] S. Adhikari, D. Sarkar, G. Madras, Hierarchical design of CuS architectures for visible
683 light photocatalysis of 4-chlorophenol, ACS omega, 2 (2017) 4009-4021.

[49] Q. Peng, H. Zhao, L. Qian, Y. Wang, G. Zhao, Design of a neutral photo-electro-Fenton system with 3D-ordered macroporous Fe_2O_3/carbon aerogel cathode: High activity and low energy consumption, Applied Catalysis B: Environmental, 174-175 (2015) 157-166.

[50] N.S. Lima, É.M. Souza, N.H. Torres, R. Bergamasco, M.N. Marques, S. Garcia-Segura, O.L. Sanchez de Alsina, E.B. Cavalcanti, Relevance of adjuvants and additives of pesticide commercial formulation on the removal performance of glyphosate by electrochemically driven processes, Journal of Cleaner Production, 212 (2019) 837-846.

[51] C. Annabi, F. Fourcade, I. Soutrel, F. Geneste, D. Floner, N. Bellakhal, A. Amrane, Degradation of enoxacin antibiotic by the electro-Fenton process: Optimization, biodegradability improvement and degradation mechanism, Journal of Environmental Management, 165 (2016) 96-105.

[52] Z.G. Li, H.J. Zhao, Decomposition of Ethanethiol by a Corona Radical Injection System, in: Materials Science Forum, Trans Tech Publ, 2018, pp. 48-53.

[53] Z. Miao, X. Gu, S. Lu, M.L. Brusseau, X. Zhang, X. Fu, M. Danish, Z. Qiu, Q. Sui, Enhancement effects of chelating agents on the degradation of tetrachloroethene in Fe(III) catalyzed percarbonate system, Chemical Engineering Journal, 281 (2015) 286-294.

[54] H. Zhao, Y. Wang, Y. Wang, T. Cao, G. Zhao, Electro-Fenton oxidation of pesticides with a novel Fe_3O_4@Fe_2O_3/activated carbon aerogel cathode: High activity, wide pH range and catalytic mechanism, Applied Catalysis B: Environmental, 125 (2012) 120-127.

[55] P. Dong, W. Liu, S. Wang, H. Wang, Y. Wang, C. Zhao, In suit synthesis of Fe_3O_4 on carbon fiber paper@polyaniline substrate as novel self-supported electrode for heterogeneous electro-Fenton oxidation, Electrochimica Acta, 308 (2019) 54-63.

[56] F. Hao, W. Guo, X. Lin, Y. Leng, A. Wang, X. Yue, L. Yan, Degradation of Acid Orange 7 in aqueous solution by dioxygen activation in a pyrite/H_2O/O_2 system, Environmental Science and Pollution Research, 21 (2014) 6723-6728.

709 [57] S.S. Abu Amr, H.A. Aziz, New treatment of stabilized leachate by ozone/Fenton in the
710 advanced oxidation process, Waste Management, 32 (2012) 1693-1698.
711 [58] Y. Shen, Q. Xu, J. Shi, M. Li, Y. Zhang, Optimization and mechanism study of CI Acid
712 Blue 25 wastewater degradation by ozone/Fenton oxidation process: response surface
713 methodology, intermediate products and degradation pathway, Desalination and Water
714 Treatment, 65 (2017) 313-326.
715 [59] Z. Xiong, B. Lai, P. Yang, Insight into a highly efficient electrolysis-ozone process for
716 N,N-dimethylacetamide degradation: Quantitative analysis of the role of catalytic ozonation,
717 fenton-like and peroxone reactions, Water Research, 140 (2018) 12-23.
718 [60] T. Le, T. Nguyen, Z. Yacouba, L. Zoungrana, F. Avril, E. Petit, J. Mendret, V. Bonniol,
719 M. Bechelany, S. Lacour, G. Lesage, M. Cretin, Toxicity removal assessments related to
720 degradation pathways of azo dyes: Toward an optimization of Electro-Fenton treatment,
721 Chemosphere, 161 (2016) 308-318.
722 [61] F. Sopaj, N. Oturan, J. Pinson, F. Podvorica, M.A. Oturan, Effect of the anode materials
723 on the efficiency of the electro-Fenton process for the mineralization of the antibiotic
724 sulfamethazine, Applied Catalysis B: Environmental, 199 (2016) 331-341.

725

726

727 **Figures captions**

728 **Fig. 1.** SEM images of CuFeNLDH (a-d), CNTs (e-h), CuFeNLDH-CNTs (i-l) and
729 CuFeNLDH-CNTs-coated graphite cathode (m-p).

730 **Fig. 2.** HR-TEM images of CuFeNLDH (a and b) and CuFeNLDH-CNTs (c and d), along with
731 thickness (e) and width (f) size distribution plots of CuFeNLDH nanosheets.

732 **Fig. 3.** XRD patterns of CuFeNLDH (a) CuFeNLDH-CNTs (b) and CuFeNLDH-CNTs
733 modified graphite (c).

734 **Fig. 4.** XPS spectra of (a) CuFeNLDH, (b) CuFeNLDH-CNTs and (c) CuFeNLDH-CNTs-
735 coated graphite; together with high resolution Fe 2p (d-f), Cu 2p (g-i) and O 1s (j-l) XPS spectra
736 of CuFeNLDH, CuFeNLDH-CNTs and CuFeNLDH-CNTs-coated graphite samples.

737 **Fig. 5.** CV scans in N_2- saturated (a) and (b) O_2-saturated solutions and LSV (b) curves for the
738 bare graphite and CuFeNLDH/CNTs-modified graphite cathodes.

739 **Fig. 6.** (a) Comparison of various graphite cathodes, including graphite/NLDH-CNTs (0.10 g),
740 graphite/NLDH-CNTs (0.05 g), graphite/NLDH-CNTs (0.15 g) and graphite/CNTs (0.10 g)
741 for the degradation of cefazolin through EF process; along with the (b) comparison of the
742 amount of H_2O_2 molecules generated on the surface of graphite/CNTs, bare graphite,
743 graphite/NLDH-CNTs (0.05 g) , graphite/NLDH-CNTs (0.10 g) and graphite/NLDH-CNTs
744 (0.15 g) electrodes (Experimental conditions: pH = 6, $[cefazolin]_0$ = 20.0 mg/L, current = 300.0
745 mA, $[Na_2SO_4]$ = 50.0 mmol/L and air flow rate = 10.0 L/h).

746 **Fig. 7.** (a) The effect of solution pH ($[cefazolin]_0$ = 20.0 mg/L, current = 400.0 mA, $[Na_2SO_4]$
747 = 50.0 mmol/L and air flow = 10.0 L/h), (b) applied current (pH = 6.0, $[cefazolin]_0$ = 20.0
748 mg/L, $[Na_2SO_4]$ = 50.0 mol/L and air flow = 10.0 L/h), (c) initial concentration of cefazolin
749 (pH = 6.0, current = 300.0 mA, $[Na_2SO_4]$ = 50.0 mmol/L and air flow = 10.0 L/h), and (d)
750 electrolyte concentration (pH = 6.0, $[cefazolin]_0$ = 20.0 mg/L, current = 300.0 mA and air flow
751 = 10.0 L/h) on the degradation of cefazolin through CuFeNLDH-CNTs/EF process.

752 **Fig. 8.** Effects of ethanol (a), benzoquinone (b), and carbonate ions (c) on the degradation of
753 cefazolin by the CuFeNLDH-CNTs/EF process. Experimental conditions: pH = 6, $[cefazolin]_0$
754 = 20.0 mg/L, current = 300.0 mA, $[Na_2SO_4]$ = 50.0 mmol/L, air flow rate = 10.0 L/h and
755 [scavenger] = 5.0-15.0 mmol/L.

Fig. 9. Effect of gas injection (air, O_2, O_3, and Ar) on the degradation of cefazolin by the CuFeNLDH-CNTs/EF process. Experimental conditions: pH = 6.0, $[cefazolin]_0$ = 20.0 mg/L, current = 300.0 mA, $[Na_2SO_4]$ = 50.0 mmol/L, gas flow rate = 10.0 L/h.

Research highlights

• Preparation of CuFeNLDH-CNTs incorporated graphite cathode.

• Study of the performance of CuFeNLDH-CNTs attached cathode in electro-Fenton process.

• Achievement of the highest cefazolin degradation through CuFeNLDH-CNTs/EF process.

• Evaluation of the effect of operational parameters on the degradation of cefazolin.

• Identification of degradation intermediates using GC-MS analysis.

Graphical abstract

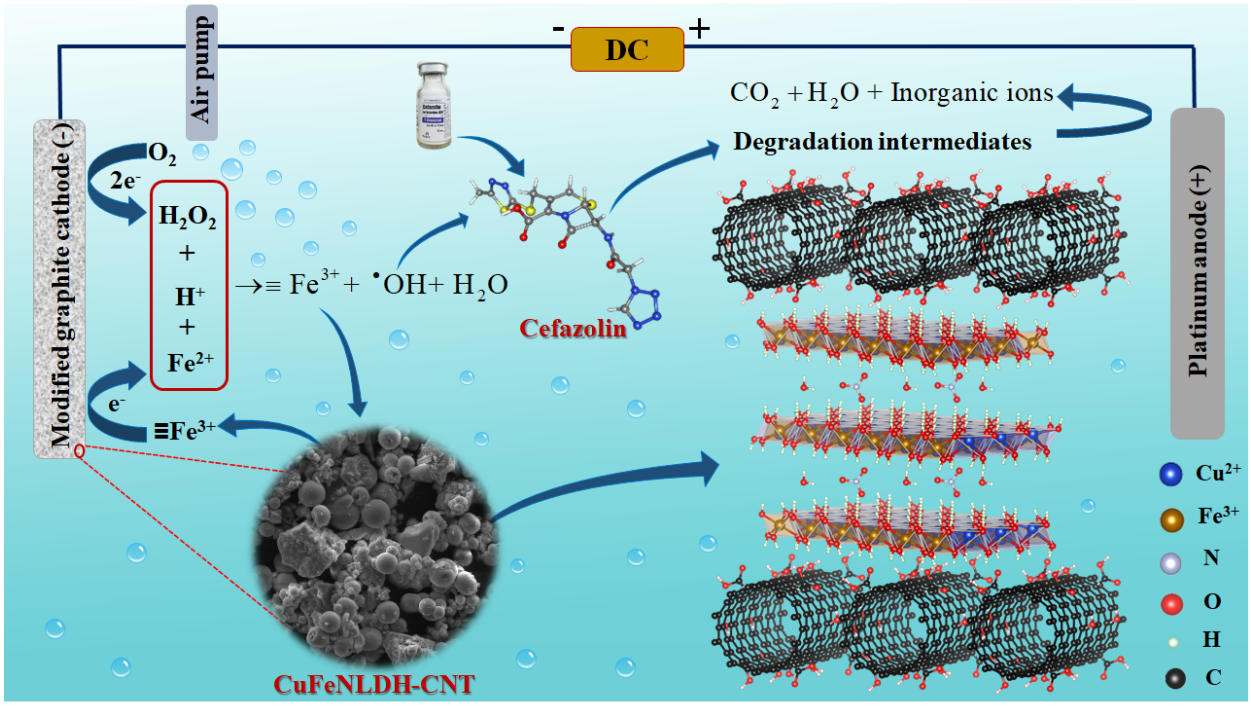

Figures

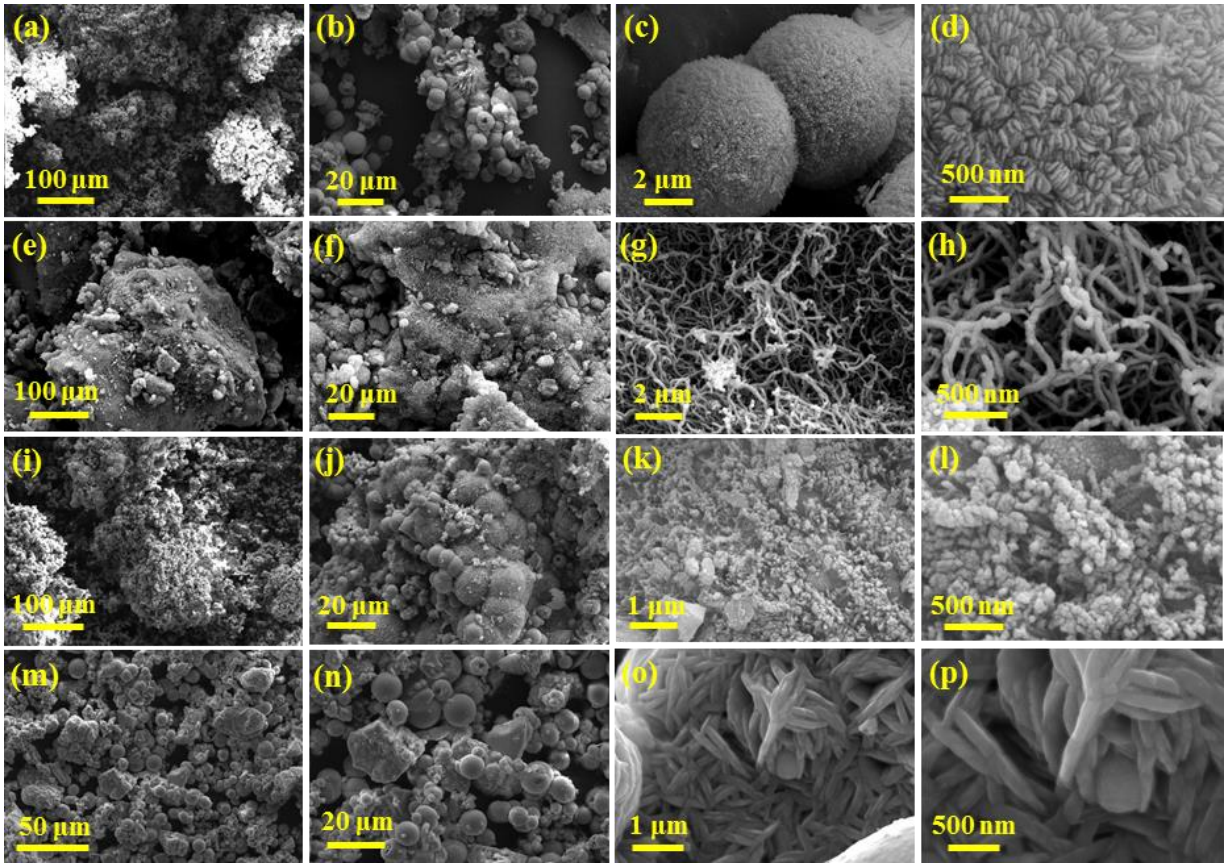

Fig. 1. SEM images of CuFeNLDH (a-d), CNTs (e-h), CuFeNLDH-CNTs (i-l) and CuFeNLDH-CNTs-coated graphite cathode (m-p).

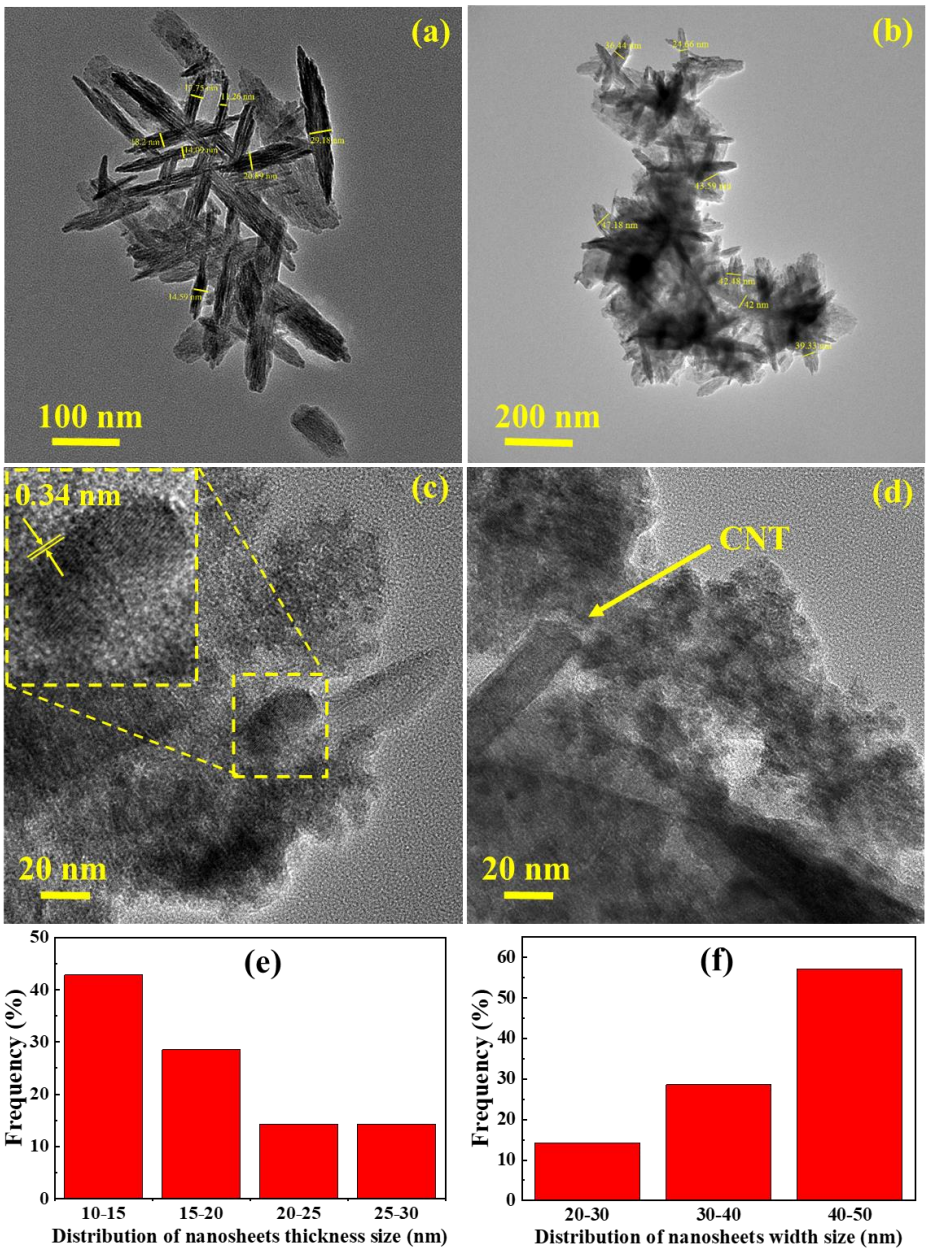

Fig. 2. HR-TEM images of CuFeNLDH (a and b) and CuFeNLDH-CNTs (c and d), along with thickness (e) and width (f) size distribution plots of CuFeNLDH nanosheets.

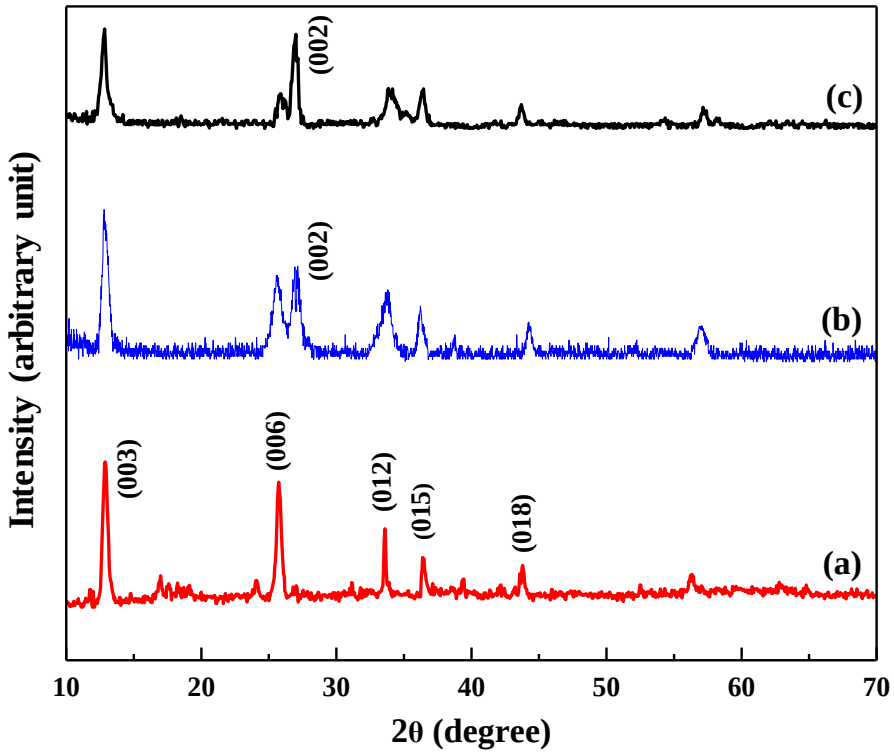

Fig. 3. XRD patterns of CuFeNLDH (a) CuFeNLDH-CNTs (b) and CuFeNLDH-CNTs modified graphite (c).

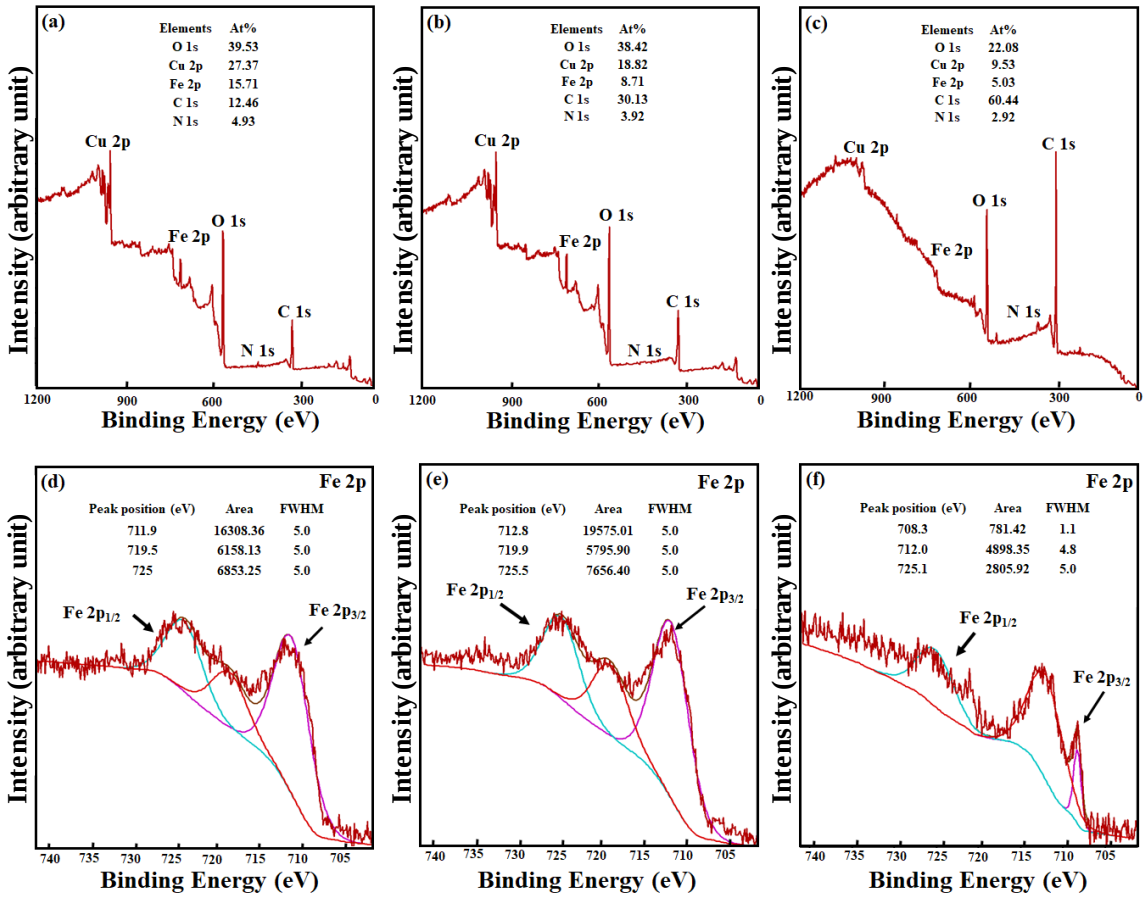
(a)
Elements At%
O 1s 39.53
Cu 2p 27.37
Fe 2p 15.71
C 1s 12.46
N 1s 4.93
Cu 2p
Fe 2p
O 1s
C 1s
N 1s
Intensity (arbitrary unit)
Binding Energy (eV)
(b)
Elements At%
O 1s 38.42
Cu 2p 18.82
Fe 2p 8.71
C 1s 30.13
N 1s 3.92
(c)
Elements At%
O 1s 22.08
Cu 2p 9.53
Fe 2p 5.03
C 1s 60.44
N 1s 2.92
(d)
Fe 2p
Peak position (eV) Area FWHM
711.9 16308.36 5.0
719.5 6158.13 5.0
725 6853.25 5.0
Fe 2p1/2
Fe 2p3/2
(e)
Fe 2p
Peak position (eV) Area FWHM
712.8 19575.01 5.0
719.9 5795.90 5.0
725.5 7656.40 5.0
(f)
Fe 2p
Peak position (eV) Area FWHM
708.3 781.42 1.1
712.0 4898.35 4.8
725.1 2805.92 5.0

Fig. 4 (a-f)

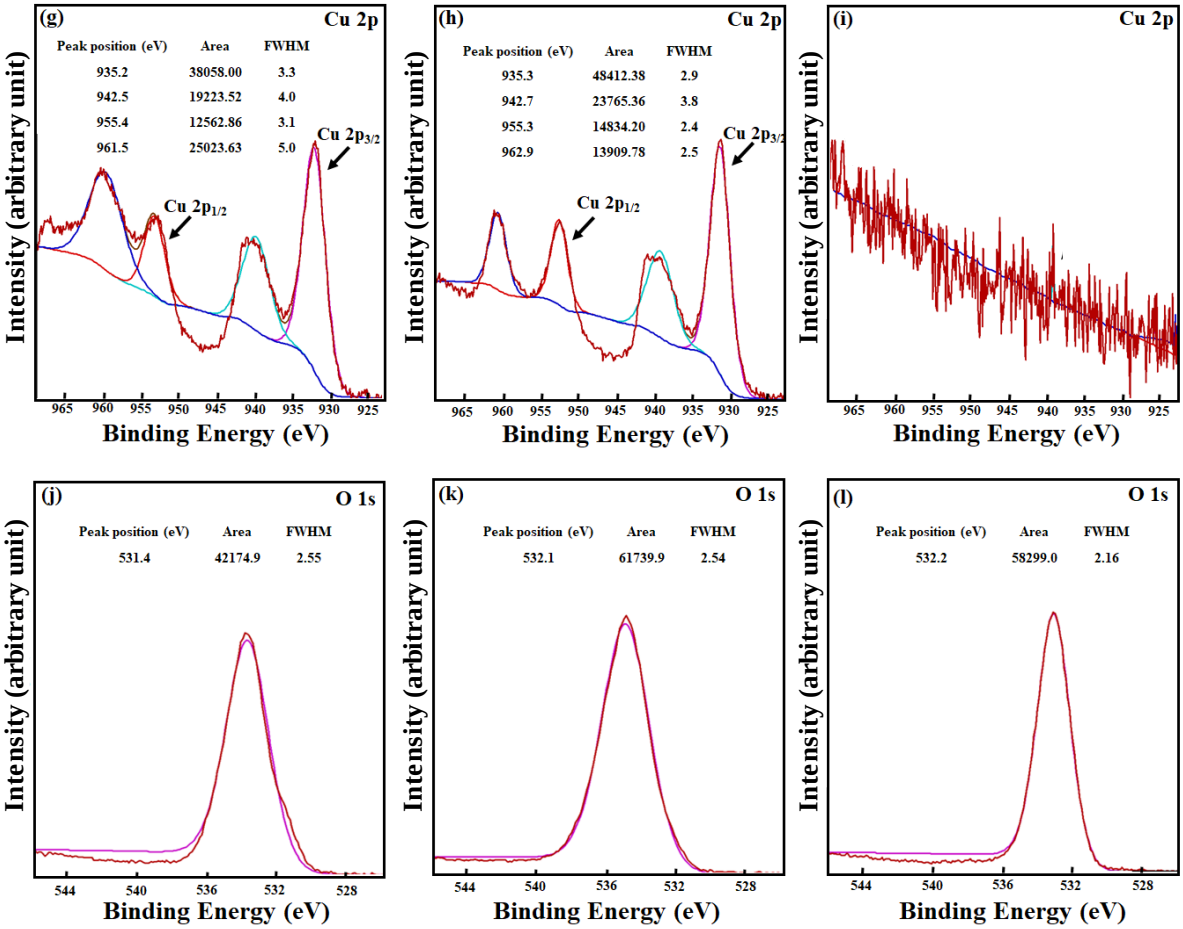

Fig. 4 (g-l)

Fig. 4. XPS spectra of (a) CuFeNLDH, (b) CuFeNLDH-CNTs and (c) CuFeNLDH-CNTs-coated graphite; together with high resolution Fe 2p (d-f), Cu 2p (g-i) and O 1s (j-l) XPS spectra of CuFeNLDH, CuFeNLDH-CNTs and CuFeNLDH-CNTs-coated graphite samples.

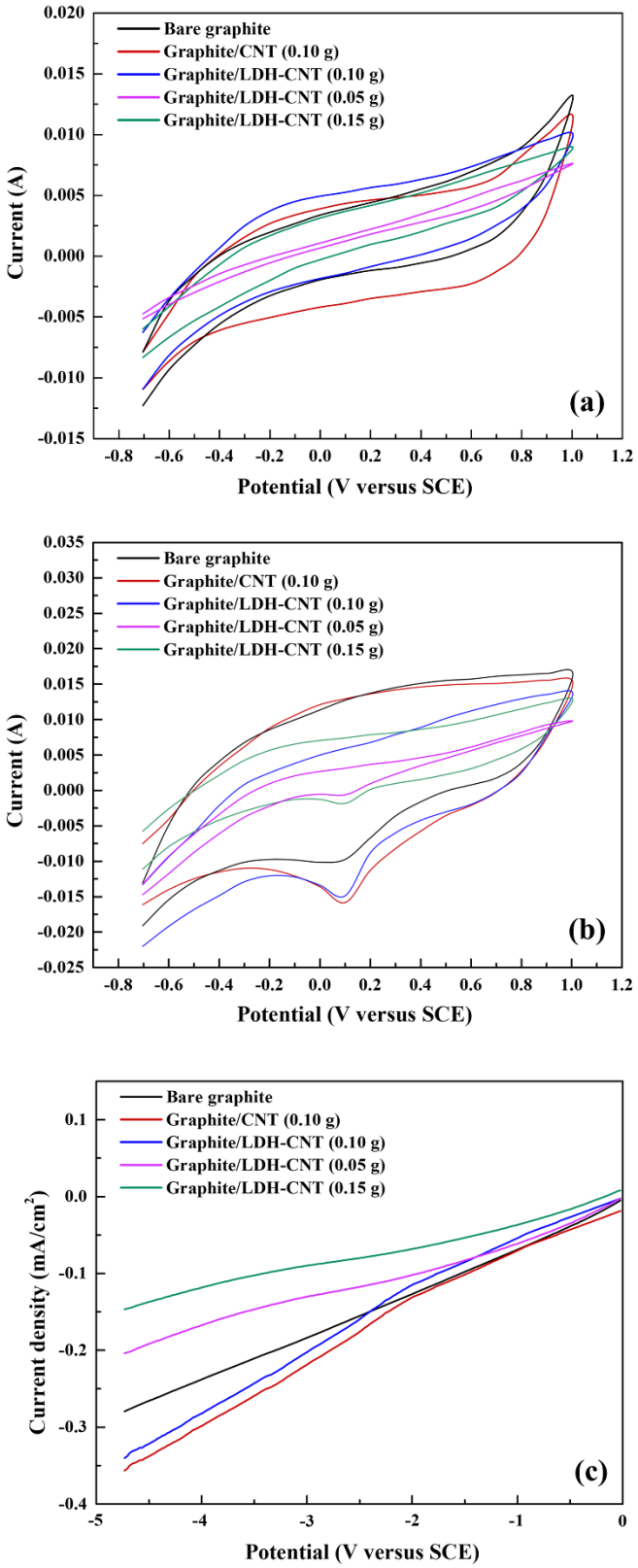

865

866

867 **Fig. 5.** CV scans in N_2-saturated (a) and O_2-saturated (b) solutions and LSV
868 curves (c) for the bare graphite and CuFeNLDH/CNTs-modified graphite
869 cathodes.

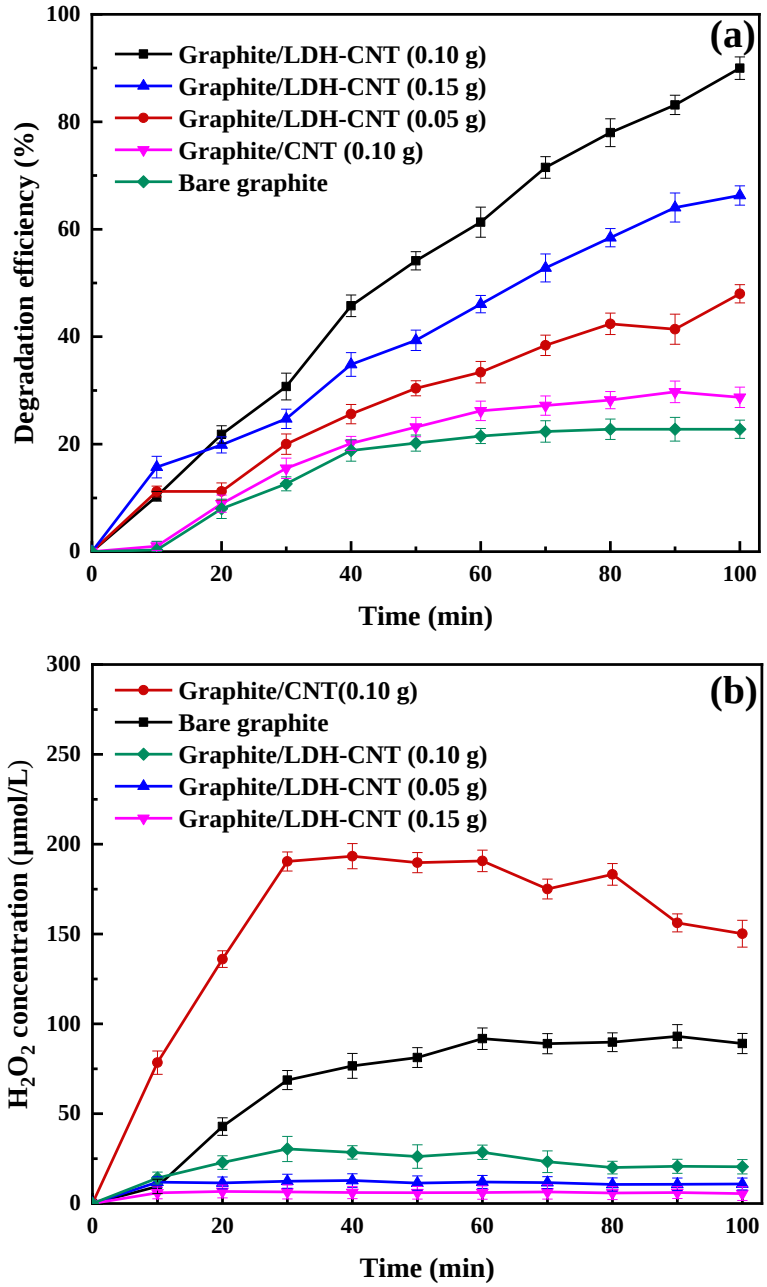

Fig. 6. (a) Comparison of various graphite cathodes, including graphite/NLDH-CNTs (0.10 g), graphite/NLDH-CNTs (0.05 g), graphite/NLDH-CNTs (0.15 g) and graphite/CNTs (0.10 g) for the degradation of cefazolin through EF process; along with the (b) comparison of the amount of H_2O_2 molecules generated on the surface of graphite/CNTs, bare graphite, graphite/NLDH-CNTs (0.05 g) , graphite/NLDH-CNTs (0.10 g) and graphite/NLDH-CNTs (0.15 g) electrodes (Experimental conditions: pH = 6, $[cefazolin]_0$ = 20.0 mg/L, current = 300.0 mA, $[Na_2SO_4]$ = 50.0 mmol/L and air flow rate = 10.0 L/h).

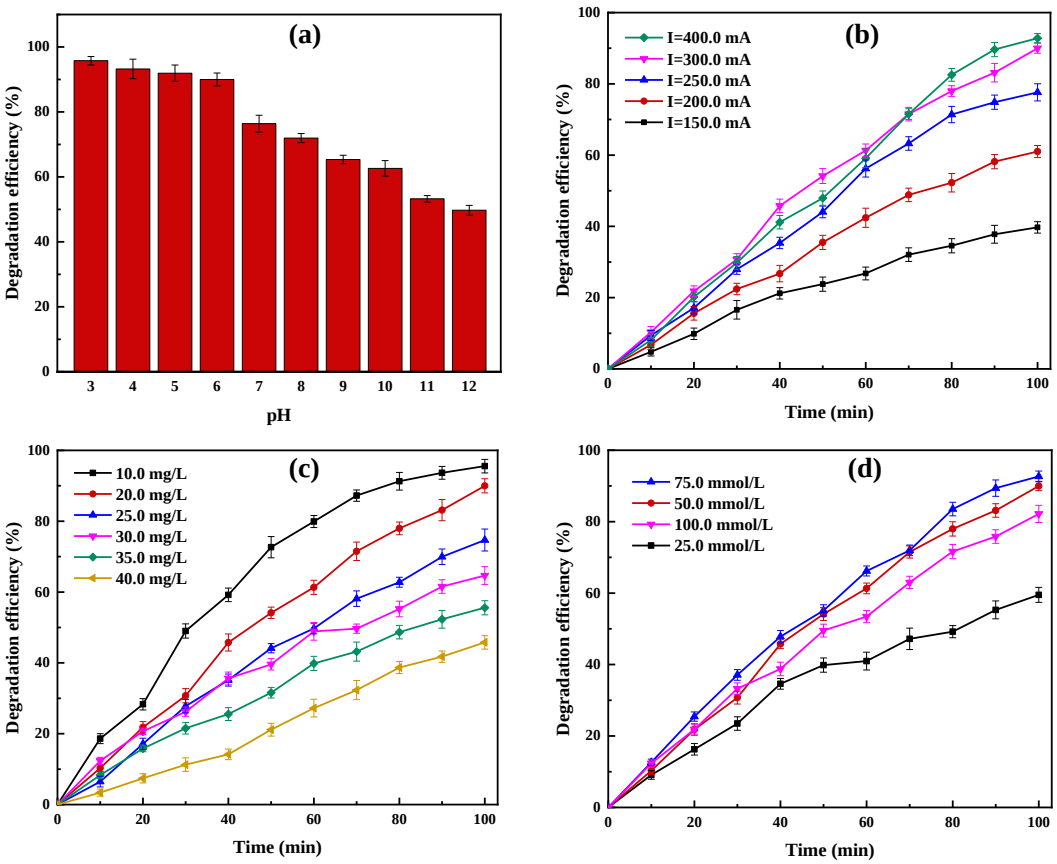

Fig. 7. (a) The effect of solution pH ([cefazolin]$_0$ = 20.0 mg/L, current = 400.0 mA, [Na_2SO_4] = 50.0 mmol/L and air flow = 10.0 L/h), (b) applied current (pH = 6.0, [cefazolin]$_0$ = 20.0 mg/L, [Na_2SO_4] = 50.0 mol/L and air flow = 10.0 L/h), (c) initial concentration of cefazolin (pH = 6.0, current = 300.0 mA, [Na_2SO_4] = 50.0 mmol/L and air flow = 10.0 L/h), and (d) electrolyte concentration (pH = 6.0, [cefazolin]$_0$ = 20.0 mg/L, current = 300.0 mA and air flow = 10.0 L/h) on the degradation of cefazolin through CuFeNLDH-CNTs/EF process.

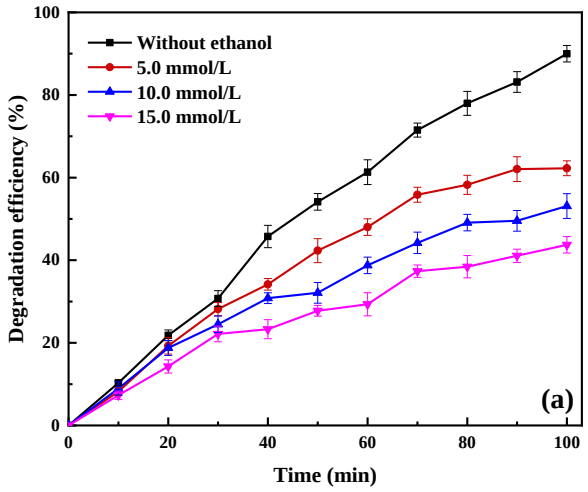

891

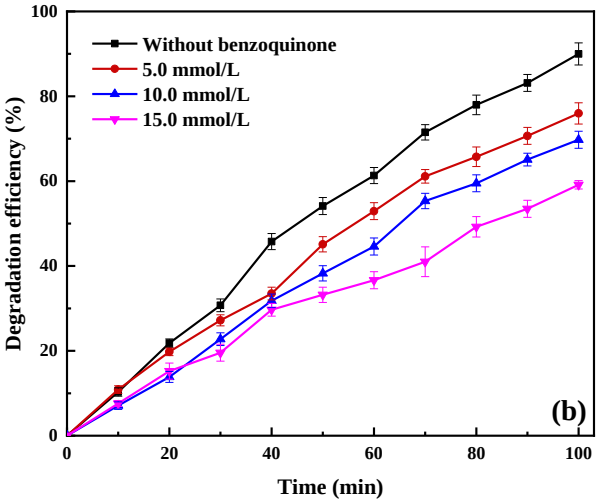

892

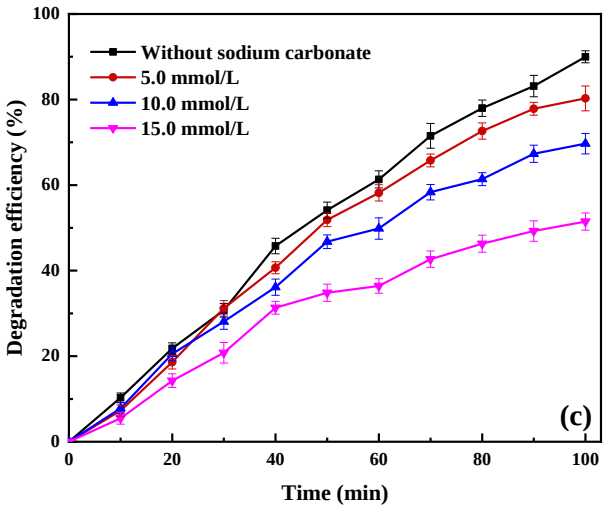

893

894 **Fig. 8.** Effects of ethanol (a), benzoquinone (b), and carbonate ions (c) on the degradation of
895 cefazolin by the CuFeNLDH-CNTs/EF process. Experimental conditions: pH = 6,
896 $[cefazolin]_0$ = 20.0 mg/L, current = 300.0 mA, $[Na_2SO_4]$ = 50.0 mmol/L, air flow rate = 10.0
897 L/h and [scavenger] = 5.0-15.0 mmol/L.
898

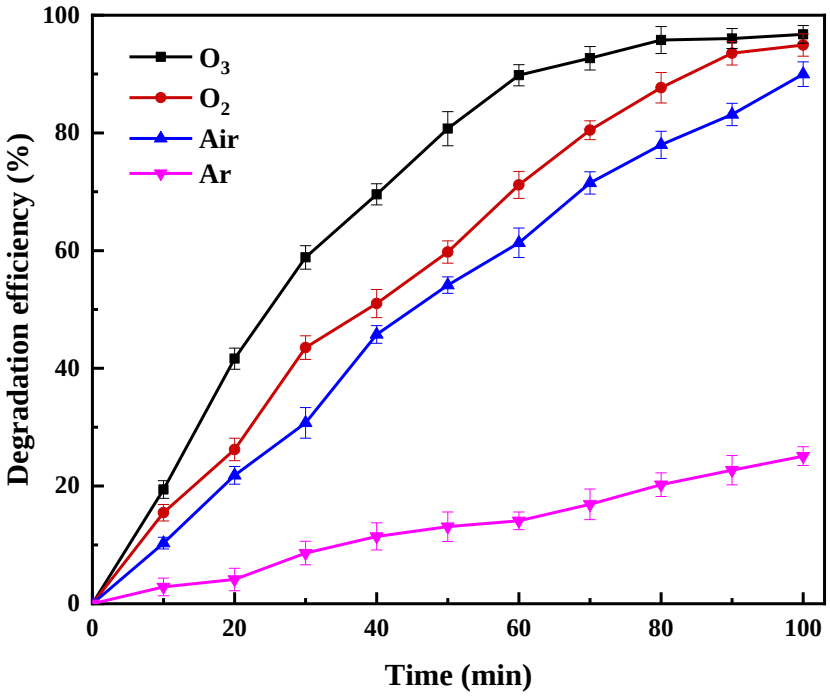

Fig. 9. Effect of gas injection (air, O_2, O_3, and Ar) on the degradation of cefazolin by the CuFeNLDH-CNTs/EF process. Experimental conditions: pH = 6.0, $[cefazolin]_0$ = 20.0 mg/L, current = 300.0 mA, $[Na_2SO_4]$ = 50.0 mmol/L, gas flow rate = 10.0 L/h.

Tables

Table 1. Characteristics of cefazolin.

Name	Chemical structure	Molecular formula	λ_{max} (nm)	M_w (g/mol)
Cefazolin	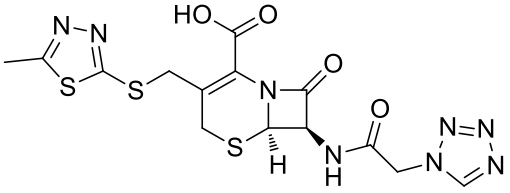	$C_{14}H_{14}N_8O_4S_3$	260	454.498

Table 2. Identified intermediate byproducts generated during the degradation of cefazolin by the heterogeneous EF process. Experimental conditions: pH = 6.0, current = 300.0 mA, [cefazolin]$_0$ = 20.0 mg/L, [Na_2SO_4] = 50.0 mmol/L, and air flow rate = 10.0 L/h.

No.	Compound name	Structure	Retention time (min)	Main fragments
1	2-(4-methyl-3-(prop-1-en-2-yl)-4-vinylcyclohexyl)propan-2-ol	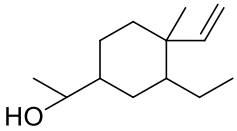	15.678	**69**, 75, 82, 93, 148
2	(2E)-3,7-dimethylocta-2,6-dien-1-ol	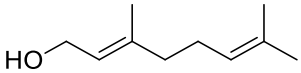	12.216	68, **69**, 121, 148
3	2-Cyclohexen-1-one, 2-methyl-5-(1-methylethenyl)-, oxime	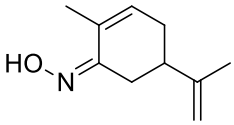	10.163	54, **82**, 93, 108, 207
4	Propan-2-ol		7.167	59, 73, **75**, 147, 187
5	Pentan-2-ol	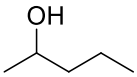	7.03	59, 75, 147, **187**
6	Octan-4-ol	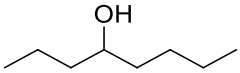	7.012	73, **75**, 147
7	1,1-bis(methylthio)ethane	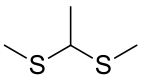	6.912	59, 73, **75**, 147, 149
8	2-Ethylcyclohexanol	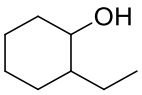	3.938	68, **69**, 93, 148
9	Acetic acid	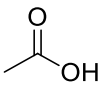	3.805	59, **75**, 76, 116
10	2-Hydroxyacetaldehyde	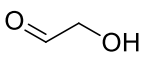	3.339	73, 75, **76**, 116

11	Acetamide	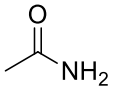	3.150	59, 73, **75**, 76, 116

Supplementary data

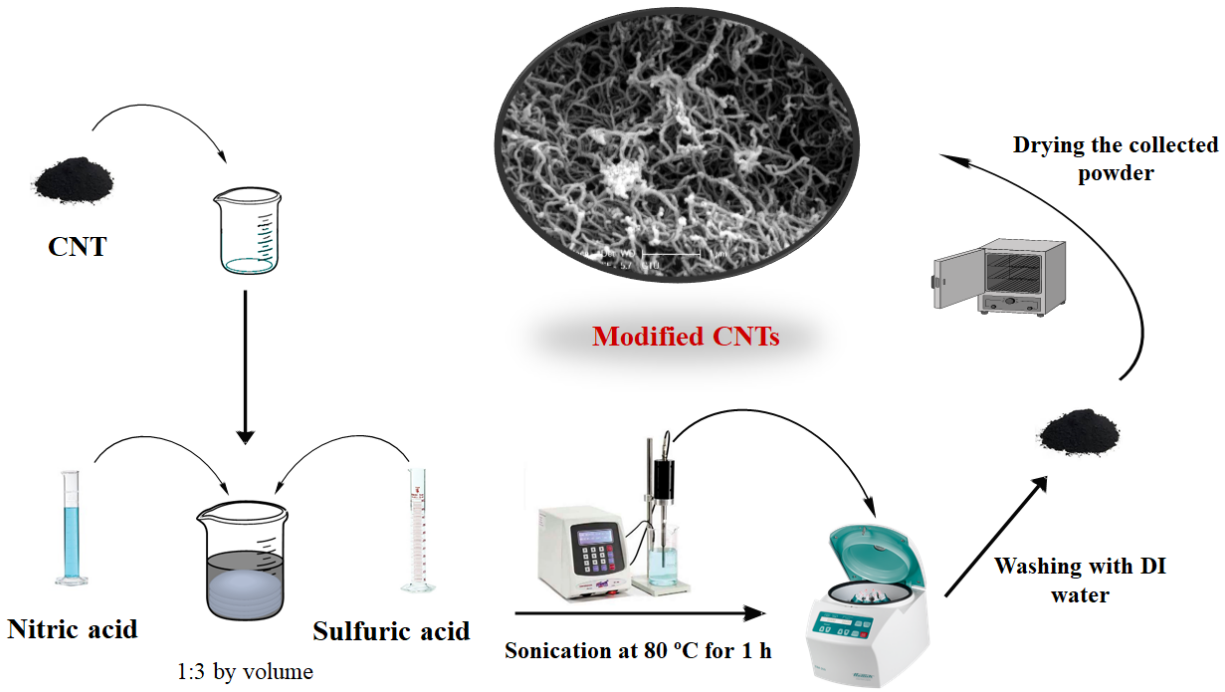

Fig. S1. Schematic design for the modification of CNTs.

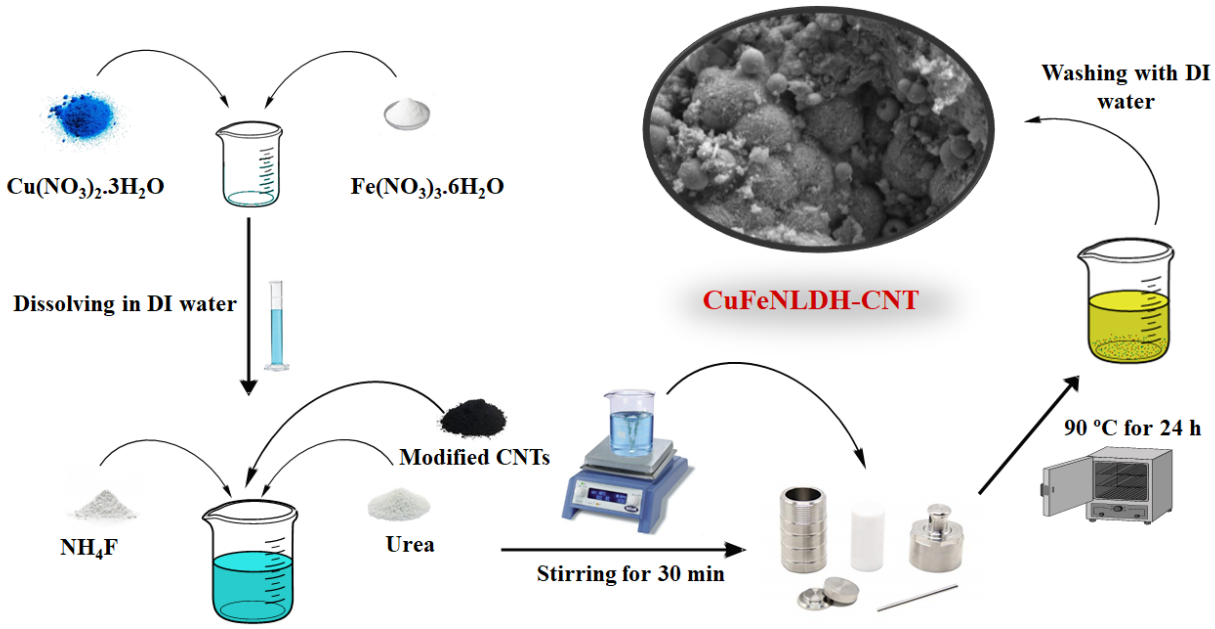

Fig. S2. Schematic diagram for synthesis of CuFeNLDH-CNTs.

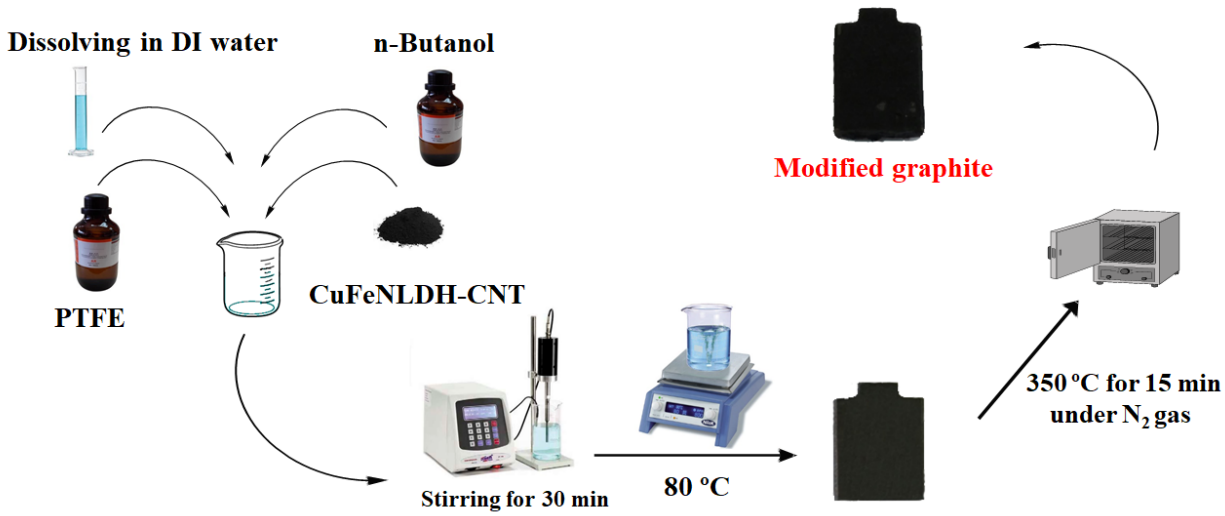

Fig. S3. Schematic diagram for immobilization of CuFeNLDH-CNTs nanocomposite on the surface of graphite plate.

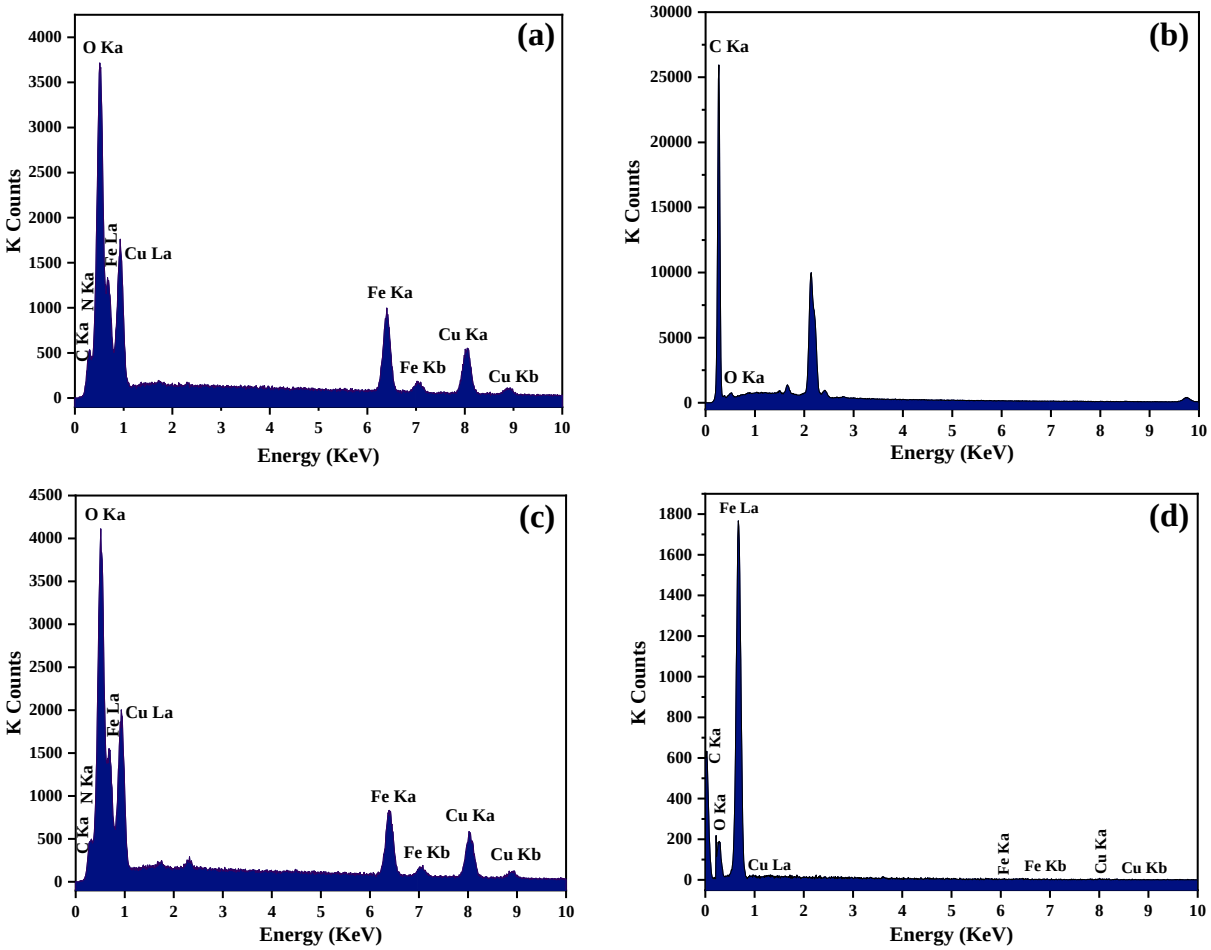

Fig. S4. EDX spectra of CuFeNLDH (a) CNTs (b), CuFeNLDH-CNTs (c) and modified graphite (d).

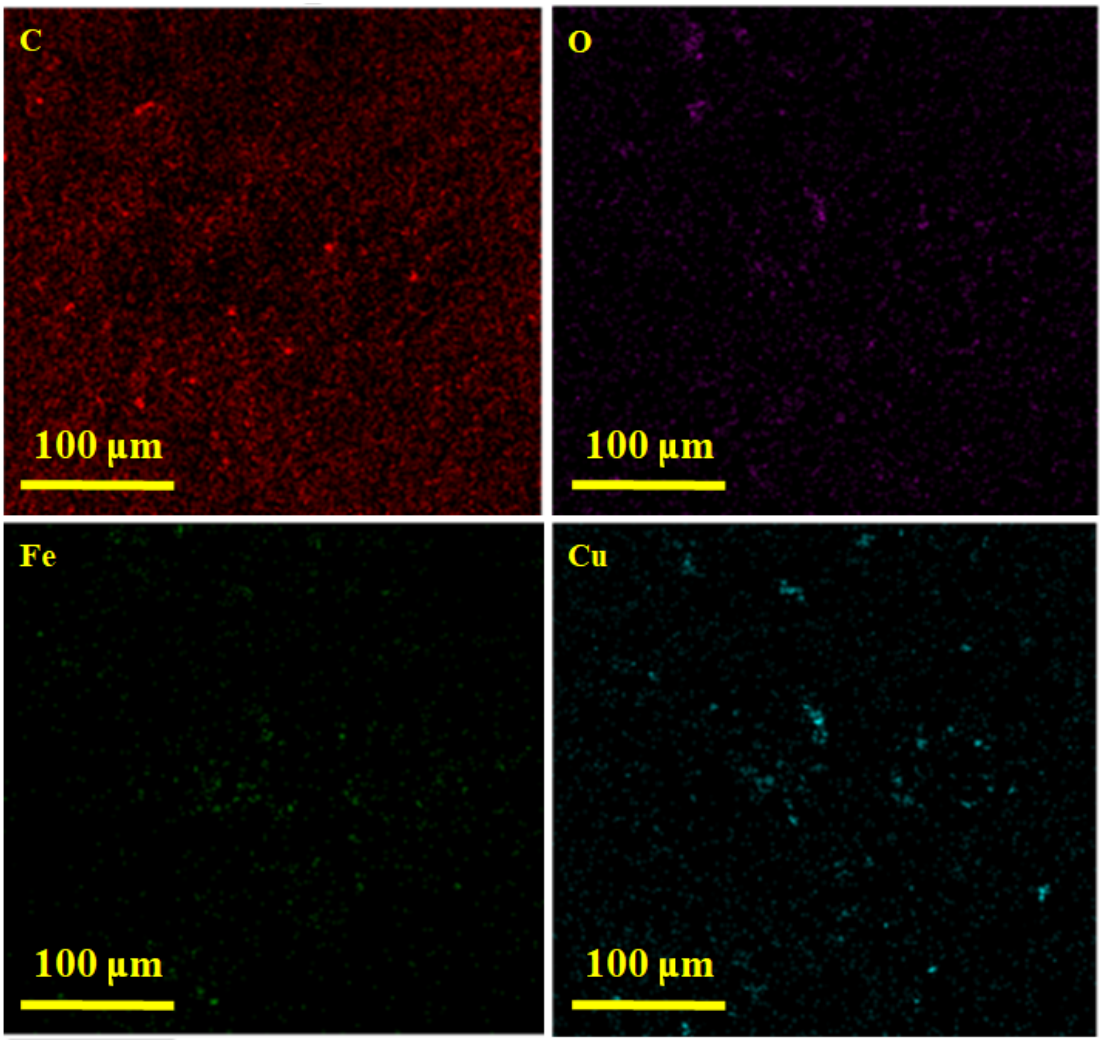

Fig. S5. Elemental mapping images of CuFeNLDH-CNTs-coated -coated graphite cathode.

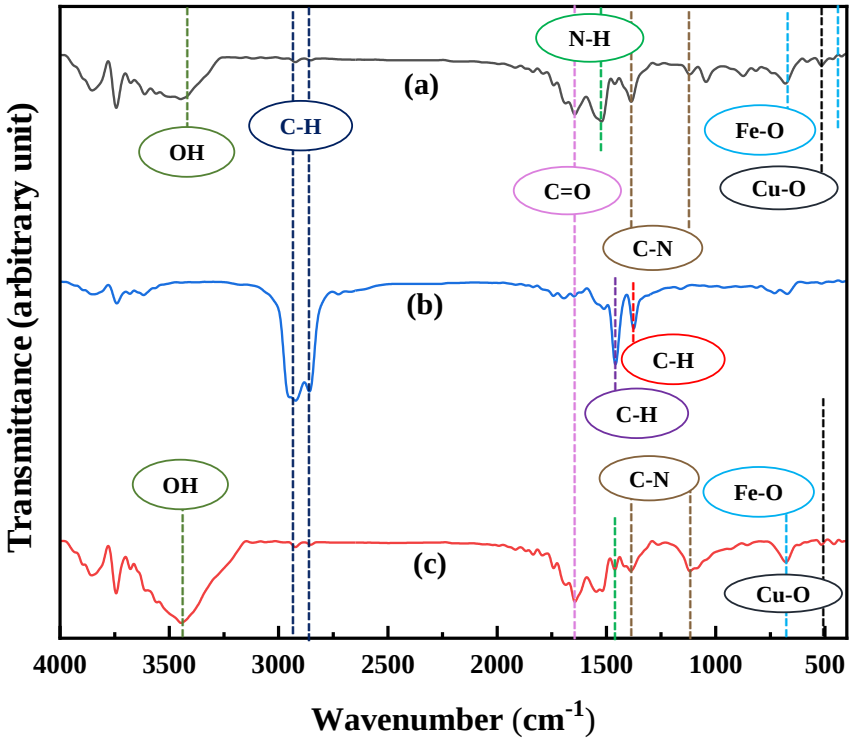

Fig. S6. FT-IR spectra of CuFeNLDH (a) CNTs (b) and CuFeNLDH/CNTs (c).

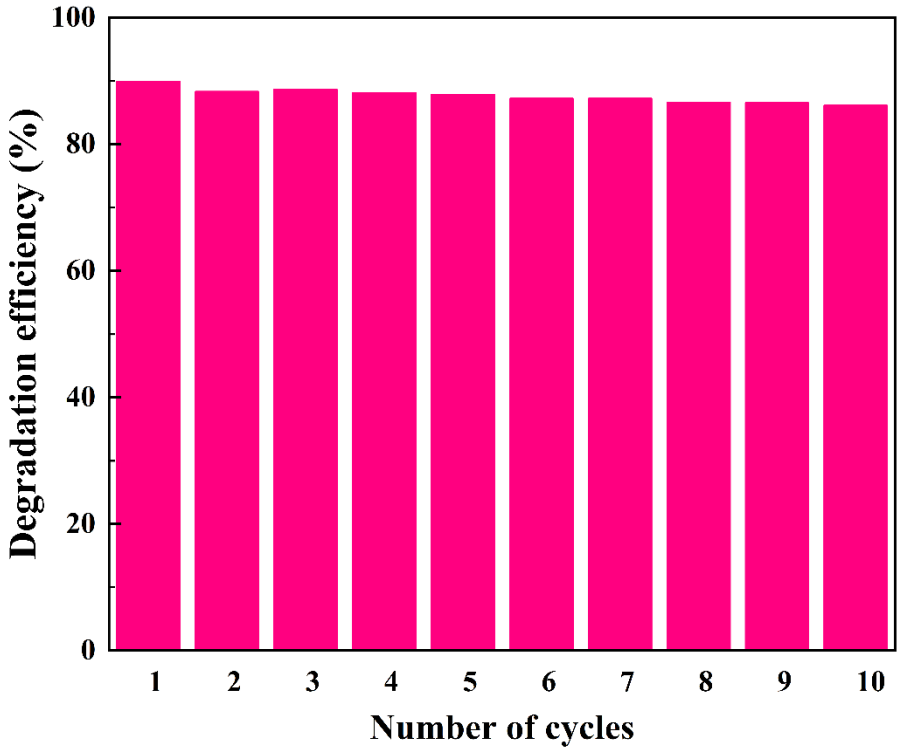

Fig. S7. Cyclic stability of CuFeNLDH-CNTs-coated graphite cathode for CFZ degradation through EF process; Experimental condition: pH = 6, $[cefazolin]_0$ = 20.0 mg/L, current = 300.0 mA, $[Na_2SO_4]$ = 0.05 mol/L and air flow rate = 10.0 L/h.